Collective Neutrino Oscillations

Huaiyu Duan,[1] George M. Fuller,[2] and Yong-Zhong Qian[3]

[1]Theoretical Division, Los Alamos National Laboratory, Los Alamos, New Mexico 87545; email: Huaiyu.Duan@MailAPS.org

[2]Department of Physics, University of California, San Diego, La Jolla, California 92093; email: gfuller@ucsd.edu

[3]School of Physics and Astronomy, University of Minnesota, Minneapolis, Minnesota 55455; email: qian@physics.umn.edu

Annu. Rev. Nucl. Part. Sci. 2010. 60:569–94

First published online as a Review in Advance on July 20, 2010

The *Annual Review of Nuclear and Particle Science* is online at nucl.annualreviews.org

This article's doi: 10.1146/annurev.nucl.012809.104524

0163-8998/10/1123-0569$20.00

Key Words

neutrino masses and mixings, neutrino spectral swaps/splits, supernova neutrino signals

Abstract

We review the rich phenomena associated with neutrino flavor transformation in the presence of neutrino self-coupling. Our exposition centers on three collective neutrino oscillation scenarios: (*a*) a simple bipolar neutrino system that initially consists of monoenergetic ν_e and $\bar{\nu}_e$, (*b*) a homogeneous and isotropic neutrino gas with multiple neutrino/antineutrino species and continuous energy spectra, and (*c*) a generic neutrino gas in an anisotropic environment. We use each of these scenarios to illustrate key facets of collective neutrino oscillations. We discuss the implications of collective neutrino flavor oscillations for core-collapse supernova physics and for the prospects of obtaining and/or constraining fundamental neutrino properties, such as the neutrino mass hierarchy and θ_{13} from a future observed supernova neutrino signal.

Contents

1. INTRODUCTION

1.1. Neutrino Mixing and Astrophysics

Neutrinos and the phenomena associated with neutrino flavor transformation stand at the nexus of two exciting recent developments: the success of experimental neutrino physics and the tremendous growth of astronomy and astrophysics. The former enterprise has provided key insights into neutrino mass and vacuum mixing and promises more (1), and the latter has provided fundamental cosmological parameters and is revealing how structure and elemental abundances emerge and evolve in the universe (2–5). Moreover, there is feedback between these subjects. For example, observations of large-scale structure and the cosmic microwave background radiation currently provide our best limits on the neutrino rest masses (6, 7). Both the early universe and the massive star core-collapse and supernova explosion environments can be dominated by neutrinos. Neutrino flavor transformation in each of these environments may give insights into astrophysics and even into fundamental neutrino properties. Obtaining these insights requires confident modeling of neutrino flavor evolution in environments where neutrino-neutrino interactions produce vexing nonlinearity. The neutrino mass and mixing data already gathered from the experiments make a compelling case that we must solve this problem.

Experiments and observations have established that the neutrino energy (mass) states $|\nu_i\rangle$ ($i = 1, 2, 3$) are not coincident with the weak interaction states $|\nu_\alpha\rangle$ ($\alpha = e, \mu, \tau$). The relation between these bases is given by $|\nu_\alpha\rangle = \sum_i U^*_{\alpha i}|\nu_i\rangle$ (8), where the Maki-Nakagawa-Sakata (MNS) matrix

elements $U_{\alpha i}$ are parameterized by three vacuum mixing angles (θ_{12}, θ_{23}, and θ_{13}) and a *CP*-violating phase (δ). Two of these, $\sin^2\theta_{12} \approx 0.31$ and $\sin^2\theta_{23} \approx 0.5$, are measured outright, whereas there is a firm upper limit on the third, $\sin^2\theta_{13} < 0.04$ at 2σ (9). Observations of solar neutrinos show flavor conversion in the $\nu_e \rightleftharpoons \nu_{\mu/\tau}$ channel with characteristic mass-squared splitting $\Delta m^2_{\odot} \approx 7.6 \times 10^{-5}\ \mathrm{eV}^2$. Atmospheric neutrino measurements show near-maximal vacuum mixing in the $\nu_\mu \rightleftharpoons \nu_\tau$ channel with corresponding mass-squared splitting $\Delta m^2_{\mathrm{atm}} \approx 2.4 \times 10^{-3}\ \mathrm{eV}^2$. However, experiments do not reveal the absolute neutrino rest masses m_i ($i = 1, 2, 3$), nor do they show whether these neutrino mass eigenvalues are ordered in the normal mass hierarchy ($m_3 > m_2 > m_1$) or in the inverted mass hierarchy ($m_2 > m_1 > m_3$).

Future terrestrial neutrino experiments (10–15) will be directed primarily toward measuring θ_{13} and, if θ_{13} is big enough, the neutrino mass hierarchy and possibly even the *CP*-violating phase δ. Planned reactor and long-baseline experiments may be able to measure θ_{13} if it satisfies $\sin^2\theta_{13} > 10^{-4}$. This limit ultimately is set by constraints on the neutrino flux and detector mass. To find significantly larger neutrino fluxes we must turn to cosmic sources, such as core-collapse supernovae (16–23).

Stars whose masses are greater than $\sim 8\, M_\odot$ end their lives in gravitational collapse and the production of a neutron star or, if they are massive enough, a black-hole remnant (24–27). Neutrinos play a role in nearly every aspect of the evolution of these core-collapse supernovae, from dominating lepton number and entropy loss from the epoch of core carbon/oxygen burning onward, to providing the bulk of energy and lepton number transport during collapse itself. Neutrinos may provide the heating necessary to engender convection (28–35) and, for instance, the standing accretion shock instability, which may create an explosion (36, 37).

A key point is that gravitational collapse causes an appreciable fraction of the rest mass of the Chandrasekhar mass ($\sim 1.4 M_\odot$) core to appear as seas of trapped neutrinos, which subsequently diffuse out of the core on timescales of seconds (38–40). At core bounce, the energy in the neutrino seas trapped in the core is $\sim 10^{52}$ ergs, but by ~ 10 s after core bounce an energy of some 10^{53} ergs, or $\sim 10\%$ of the rest mass of the core, has been radiated away as neutrinos of all kinds. The emergent neutrino and antineutrino energy spectra and fluxes at the neutrino sphere vary with time post–core bounce, but there are epochs in which the energy spectra and/or the luminosities in the various neutrino flavors differ. Moreover, charged-current, flavor-specific neutrino interaction processes such as $\nu_e + n \rightleftharpoons p + e^-$ and $\bar{\nu}_e + p \rightleftharpoons n + e^+$ are important both for energy and electron lepton number deposition as well as for determining neutrino transport physics (41–43). It is therefore interesting and necessary to assess whether interconversion of neutrino flavors in the supernova environment affects explosion physics and neutrino-heated nucleosynthesis and how such flavor transformation might affect a supernova neutrino burst signature in a terrestrial detector.

1.2. Brief History of Collective Neutrino Oscillations

Early studies of neutrino flavor transformation centered on solar neutrinos, especially after it was recognized first by Wolfenstein (44), and then by Mikheyev & Smirnov (45), that the medium through which the neutrino propagates could alter the effective neutrino mass and mixing properties. Almost immediately after the Mikheyev-Smirnov-Wolfenstein (MSW) mechanism was understood, it was realized that the forward coherent scattering of neutrinos with other neutrinos, somewhat misleadingly termed neutrino self-coupling or neutrino self-interaction, could generate a similar effect (46, 47). Subsequently, the effects of neutrino self-interaction were investigated independently in the core-collapse supernova and the early universe scenarios. The studies of the supernova environment first focused on MSW-like effects (41, 46, 48–51). However, the neutrino self-interaction potential is very different from the matter potential in

that it can have nonvanishing off-diagonal elements in the interaction basis (52, 53). Studies using the complete neutrino self-interaction potential showed that neutrinos could experience self-maintained coherent oscillations or collective oscillations in lepton-degenerate early universe scenarios (54–64). By collective oscillations we mean a significant fraction of neutrinos oscillating coherently with respect to one another.

Early research on MSW-like evolution, where the flavor off-diagonal potentials were minimal, as well as the first paper (65) to point out that collective effects could occur in supernovae, focused on relatively large neutrino mass–squared differences. However, neutrinos and antineutrinos can be transformed collectively and simultaneously even for the small, measured neutrino mass–squared differences (66, 67). Additionally, ordinary matter does not necessarily suppress collective neutrino oscillations, at least in homogeneous and isotropic environments (68). As a consequence, collective neutrino oscillations may occur deep in the envelope of a supernova (69, 70). These studies showed that the neutrino energy spectra would be modified differently for the normal and inverted neutrino mass hierarchies (**Figure 1**).

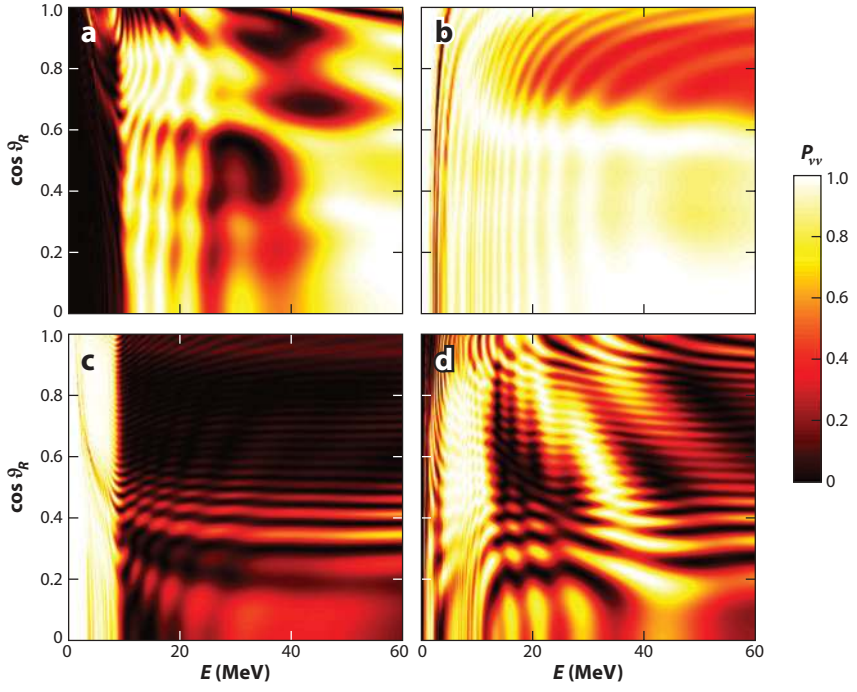

Figure 1

Survival probabilities $P_{\nu\nu}$ for (*a*,*c*) neutrinos and (*b*,*d*) antineutrinos as functions of both neutrino energy E and emission angle ϑ_R in a numerical calculation using the neutrino bulb model (see **Figure 3**) and the two-flavor mixing scheme. The most prominent features are (*a*,*c*) the approximately angle-independent step-like changes in the neutrino survival probabilities—these are the spectral swaps/splits first shown in Reference 70. The energy spectra of ν_e and ν_μ with energy below (above) $E \simeq 9$ MeV in this calculation are almost completely swapped in panel *a* (*c*), which employs the normal (inverted) neutrino mass hierarchy. Spectral swaps/splits are the result of a collective neutrino oscillation mode known as the precession mode. The vertical fringes (the energy-dependent features in the figure) are the result of Mikheyev-Smirnov-Wolfenstein flavor transformation, which is energy dependent. The horizontal fringes (the angle-dependent features) are the result of the kinematic decoherence of bipolar neutrino oscillations (72). The movie version of these calculations is available in Reference 87. Figure adapted from figure 3 of Reference 69.

Over the past few years, many papers have been written on the collective neutrino oscillation phenomenon and its physical effects (71–111). Following this literature can be bewildering. For example, synchronized and bipolar neutrino oscillations are frequently perceived as the two most important collective neutrino oscillation modes in supernovae. However, numerical studies suggest that supernova neutrinos are probably never synchronized because of the nonvanishing matter density (76), and the bipolar oscillation is not a collective neutrino oscillation mode in anisotropic environments such as supernovae (72).

1.3. Goal and Organization of This Review

The purpose of this review is to provide a relatively short but in-depth exposition of the properties of collective neutrino oscillations that are reasonably well understood. Specifically, we elucidate the physics behind striking features such as the swaps of supernova neutrino energy spectra caused by collective oscillations, as shown in **Figure 1**. Our strategy is to illustrate key facets of collective neutrino oscillations by describing three increasingly complex models.

The rest of the review is organized as follows. In Section 2 we try to make the connection between the so-called wave function language and the spin language, which are commonly used for studying noncollective and collective neutrino oscillations, respectively. In Section 3 we discuss the flavor evolution of a homogeneous and isotropic neutrino gas that consists initially of monoenergetic, pure ν_e and $\bar{\nu}_e$. This simple model can be solved analytically and offers important insights into the behavior of more complicated systems. In Section 4 we discuss homogeneous and isotropic gases that consist of neutrinos with continuous energy spectra. We explore adiabatic solutions to the neutrino flavor evolution equations and demonstrate how the spectral swap/split phenomenon can be explained by one of these solutions. In Section 5 we discuss some of the important neutrino oscillation properties that are unique to anisotropic environments and explain why the spectral swap/split phenomenon may occur in these environments despite the anisotropy in neutrino fields. In Section 6 we apply the current understanding of the collective neutrino oscillation phenomenon to supernova environments. In Section 7 we give a summary and identify several issues in collective neutrino oscillations that remain to be understood.

2. NEUTRINO MIXING IN DENSE NEUTRINO GASES

2.1. Equations of Motion

Here we focus on two-flavor neutrino mixing scenarios, namely $\alpha = e, \mu$ and $i = 1, 2$, where $|\nu_\mu\rangle$ is a linear combination of the physical $|\nu_\mu\rangle$ and $|\nu_\tau\rangle$. We do this for pedagogical purposes, although our choice is physically justifiable because the physical ν_μ and ν_τ are nearly maximally mixed in vacuum and experience nearly identical interactions in the supernova environment (112, 113). We discuss collective neutrino oscillations with the full three-flavor mixing machinery in Section 4.3.

We consider only coherent neutrino flavor evolution, in which the effects of neutrino inelastic scattering and associated quantum decoherence can be neglected. This is generally applicable in the region well above the neutron star in supernova models. [Solution of the complete problem of neutrino flavor evolution with both elastic and inelastic neutrino scattering would necessitate the use of the full quantum kinetic equations (7, 43, 114–116).] We also assume that neutrinos are relativistic and that general relativistic effects can be ignored. With these assumptions, a mean-field Schrödinger-like equation,

$$\mathrm{i}\frac{\mathrm{d}}{\mathrm{d}x}\psi = \mathsf{H}\psi, \qquad 1.$$

is taken to describe flavor evolution along a neutrino world line (117). Here $\hbar = c = 1$, x is the distance along the world line of the neutrino; ψ is the neutrino flavor wave function, taken to be a vector in (neutrino) flavor space; and

$$\mathsf{H} = \frac{\Delta m^2}{2E}\mathsf{B} + \lambda\mathsf{L} + \mathsf{H}_{\nu\nu} = \frac{\Delta m^2}{2E}\mathsf{B} + \sqrt{2}G_{\rm F}n_e\mathsf{L} + \sqrt{2}G_{\rm F}\int \mathrm{d}^3\mathbf{p}'(1 - \hat{\mathbf{p}}\cdot\hat{\mathbf{p}}')(\rho_{\mathbf{p}'} - \bar{\rho}_{\mathbf{p}'}) \qquad 2.$$

is the Hamiltonian. (See References 118–122 for discussions of the applicability of the one-particle effective approximation assumed in Equation 1.) The wave function for an antineutrino also obeys Equation 1, but with the replacements $\lambda \to -\lambda$ and $\mathsf{H}_{\nu\nu} \to -\mathsf{H}^*_{\nu\nu}$ in Equation 2. The flavor space is spanned by the neutrino interaction basis or, equivalently, by the mass basis. We use the word flavor in a more general sense, and we avoid using the phrase flavor state, which in the literature can mean either the interaction state $|\nu_\alpha\rangle$ or the flavor quantum state $|\psi\rangle$. (We use symbols in sans serif font, such as H, to denote basis-dependent matrices in flavor space.)

The first term in Equation 2 induces neutrino flavor transformation because in the interaction basis,

$$\mathsf{B} = \mathsf{U}\left(\frac{1}{2}\mathrm{diag}[-1, 1]\right)\mathsf{U}^\dagger = \frac{1}{2}\begin{bmatrix} -\cos 2\theta_{\rm v} & \sin 2\theta_{\rm v} \\ \sin 2\theta_{\rm v} & \cos 2\theta_{\rm v} \end{bmatrix} \qquad 3.$$

is nondiagonal. In Equation 3, U is the MNS matrix and $\theta_{\rm v}$ is the so-called vacuum mixing angle within the range $(0, \pi/4]$. In Equation 2, Δm^2 is the mass-squared difference appropriate for $|\nu_2\rangle$ and $|\nu_1\rangle$, and E is the energy of the neutrino. Here $\Delta m^2 > 0$ and $\Delta m^2 < 0$ correspond to the normal neutrino mass hierarchy (NH) and the inverted neutrino mass hierarchy (IH), respectively, as discussed above for the full three-flavor mixing case. Although this formalism is completely general, one of the most interesting supernova cases is where $|\Delta m^2| \simeq \Delta m^2_{\rm atm}$ and $\theta_{\rm v} \simeq \theta_{13} \ll 1$.

The second term in Equation 2 arises from coherent neutrino-electron forward exchange scattering (44). In this term, which is referred to as the matter term, $G_{\rm F}$ is the Fermi constant, n_e is the net electron number density, and $\mathsf{L} = \mathrm{diag}[1, 0]$ in the interaction basis. Note that adding or subtracting a multiple of the identity matrix to or from H (e.g., the contribution of neutral-current neutrino-electron scattering) gives only an overall phase to ψ and, therefore, does not affect neutrino oscillations.

The last term in Equation 2 stems from coherent neutral-current neutrino-neutrino forward exchange scattering (46–48, 52), where $\hat{\mathbf{p}}$ and $\hat{\mathbf{p}}'$ are the unit vectors for the propagation directions of the test neutrino and the background neutrino or antineutrino, respectively. In the interaction basis, at location $\mathbf{x}$ and at time t, the (flavor) density matrices for neutrinos and antineutrinos with momentum $\mathbf{p}'$ and with our assumptions can be written as

$$[\rho_{\mathbf{p}'}(t, \mathbf{x})]_{\alpha\beta} = \sum_{\nu'} n_{\nu',\mathbf{p}'}(t, \mathbf{x})\langle\nu_\alpha|\psi_{\nu',\mathbf{p}'}(t, \mathbf{x})\rangle\langle\psi_{\nu',\mathbf{p}'}(t, \mathbf{x})|\nu_\beta\rangle \qquad 4a.$$

and

$$[\bar{\rho}_{\mathbf{p}'}(t, \mathbf{x})]_{\beta\alpha} = \sum_{\bar{\nu}'} n_{\bar{\nu}',\mathbf{p}'}(t, \mathbf{x})\langle\bar{\nu}_\alpha|\psi_{\bar{\nu}',\mathbf{p}'}(t, \mathbf{x})\rangle\langle\psi_{\bar{\nu}',\mathbf{p}'}(t, \mathbf{x})|\bar{\nu}_\beta\rangle, \qquad 4b.$$

respectively, where $|\psi_{\nu'(\bar{\nu}'),\mathbf{p}'}\rangle$ is the state of a neutrino ν' (antineutrino $\bar{\nu}'$) with momentum $\mathbf{p}'$ and $n_{\nu',\mathbf{p}'}$ ($n_{\bar{\nu}',\mathbf{p}'}$) is the corresponding number density of the neutrino (antineutrino). Note that the order of the indices on the matrix representation of $\bar{\rho}$ in Equation 4*b* follows the convention in Reference 114. The advantage of this definition is that $\bar{\rho}$ transforms in the same way as does ρ when transforming from the interaction basis to the mass basis or vice versa.

2.2. Neutrino Flavor Polarization Vector

It becomes more difficult to analyze neutrino oscillations using the wave function formalism when $\mathsf{H}_{\nu\nu}$ is significant because $\mathsf{H}_{\nu\nu}$ is a sum of density matrices that involve bilinear forms of the wave functions. The density matrices contain all the physical information about the neutrino mixing problem. The diagonal elements of the density matrices give the number densities of neutrinos in the weak interaction states or the mass states, depending on the basis used, and the off-diagonal elements of the density matrices contain the neutrino mixing information. For simplicity let us first take a working example, a homogeneous and isotropic neutrino gas whose flavor content can vary with time t. Homogeneity and isotropy imply that the factor $(1-\hat{\mathbf{p}}\cdot\hat{\mathbf{p}}')$ in Equation 2 averages to one. Therefore, the neutrino propagation direction does not matter, and $\rho_{\mathbf{p}}(t,\mathbf{x}) \to \rho_E(t)$ and $\bar{\rho}_{\mathbf{p}}(t,\mathbf{x}) \to \bar{\rho}_E(t)$. These density matrices obey the equations of motion (EoMs)

$$\mathrm{i}\dot{\rho}_E = \left[\frac{\Delta m^2}{2E}\mathsf{B} + \lambda\mathsf{L} + \sqrt{2}G_{\mathrm{F}}\int_0^\infty \mathrm{d}E'(\rho_{E'} - \bar{\rho}_{E'}),\, \rho_E\right] \qquad 5a.$$

and

$$\mathrm{i}\dot{\bar{\rho}}_E = \left[-\frac{\Delta m^2}{2E}\mathsf{B} + \lambda\mathsf{L} + \sqrt{2}G_{\mathrm{F}}\int_0^\infty \mathrm{d}E'(\rho_{E'} - \bar{\rho}_{E'}),\, \bar{\rho}_E\right]. \qquad 5b.$$

Because ρ_E and $\bar{\rho}_E$ are 2×2 Hermitian matrices, they can be mapped into vectors in a three-dimensional Euclidean space, which we also refer to as flavor space. We define the components of the (neutrino flavor) polarization vector $\vec{P}_\omega$ to be

$$P_{\omega,a} = \left(\frac{1}{n_\nu}\right)\left(\frac{|\Delta m^2|}{2\omega^2}\right) \times \begin{cases} \mathrm{Tr}(\rho_E\sigma_a) & \text{for neutrinos,} \\ -\mathrm{Tr}(\bar{\rho}_E\sigma_a) & \text{for antineutrinos,} \end{cases} \qquad 6.$$

where the (angular) vacuum oscillation frequency is $\omega = \frac{\Delta m^2}{2E}$ for neutrinos and $\frac{\Delta m^2}{(-2E)}$ for antineutrinos, and σ_a ($a = 1, 2, 3$) are the Pauli matrices. (We use symbols with the vector hat, such as $\vec{P}$, to denote vectors in flavor space and symbols in the bold font, such as $\mathbf{p}$, to denote vectors in physical three-dimensional coordinate space.) Note that $\vec{P}_\omega$ can be normalized by an arbitrary factor. For example, if $\vec{P}_\omega$ is normalized to unity, then $\rho_E \propto (1 + \frac{1}{2}\vec{P}_\omega\cdot\vec{\sigma})$ for neutrinos and $\bar{\rho}_E \propto (1 - \frac{1}{2}\vec{P}_\omega\cdot\vec{\sigma})$ for antineutrinos. In Equation 6 we defined $\vec{P}_\omega$ to be normalized by n_ν, the initial total number density of a certain neutrino species ν, which is chosen to be $\bar{\nu}_e$ in the rest of this review. However, we usually take $\mu = \sqrt{2}G_{\mathrm{F}}n_\nu$ as a measure of the strength of neutrino self-interaction. Therefore, in some cases it is more appropriate to normalize $\vec{P}_\omega$ by the number density of other neutrino species, for instance, when $n_{\bar{\nu}_e}$ is negligible. If all neutrinos and antineutrinos are in the interaction states, then $\vec{P}_\omega \propto (n_{\nu_e,\omega} - n_{\nu_\mu,\omega})\hat{e}_3^{(\mathrm{I})}$ for neutrinos and $\vec{P}_\omega \propto -(n_{\bar{\nu}_e,\omega} - n_{\bar{\nu}_\mu,\omega})\hat{e}_3^{(\mathrm{I})}$ for antineutrinos, where $n_{\nu,\omega}$ ($\nu = \nu_e, \nu_\mu, \bar{\nu}_e, \bar{\nu}_\mu$) is the corresponding number density in the neutrino or antineutrino mode ω, and $\hat{e}_3^{(\mathrm{I})}$ is one of the interaction-basis vectors.

Because the Pauli matrices are traceless, the trace of the density matrix is not contained in the polarization vector. According to Equation 5, the traces of the density matrices do not change with time. (This corresponds to one of our assumptions that neutrinos are not created or annihilated.) These terms can be easily reintroduced in, for example, the calculation of the neutrino energy spectra. Use of Equations 5 and 6 shows that

$$\dot{\vec{P}}_\omega = (\omega\vec{B} + \lambda\vec{L} + \mu\vec{D}) \times \vec{P}_\omega, \qquad 7.$$

where vectors $\vec{B} = \mathrm{Tr}(\mathsf{B}\vec{\sigma})$ and $\vec{L} = \mathrm{Tr}(\mathsf{L}\vec{\sigma})$ are parallel to the (vacuum) mass and interaction-basis vectors $\hat{e}_3^{(\mathrm{V})}$ and $\hat{e}_3^{(\mathrm{I})}$, respectively (**Figure 2**), and $\vec{D} = \int_{-\infty}^{\infty}\vec{P}_\omega\,\mathrm{d}\omega$ is the total polarization vector. In the absence of neutrino self-coupling, $\vec{P}_\omega$ can be considered a "magnetic spin." In this analogy, the "magnetic spin" is coupled to two "magnetic fields," $\vec{B}$ and $\vec{L}$, with gyromagnetic

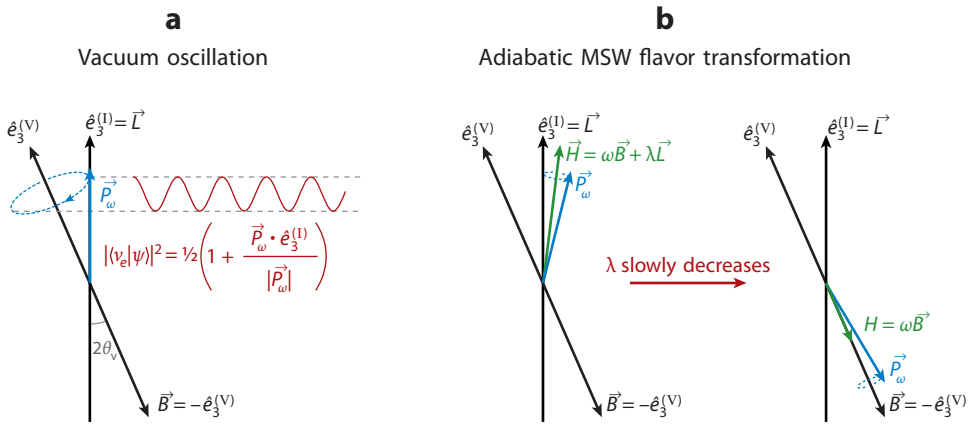

Figure 2

Geometric pictures for (*a*) vacuum oscillation and for (*b*) Mikheyev-Smirnov-Wolfenstein (MSW) flavor transformation. The flavor Hilbert space spanned by $|\nu_\alpha\rangle$ ($\alpha = e, \mu$) or $|\nu_i\rangle$ ($i = 1, 2$) can be mapped onto the flavor Euclidean space that is spanned by $\hat{e}_a^{(I)}$ or $\hat{e}_a^{(V)}$ ($a = 1, 2, 3$). The interaction-basis vectors $\hat{e}_{1,3}^{(I)}$ can be obtained by rotating the (vacuum) mass-basis vectors $\hat{e}_{1,3}^{(V)}$ by $2\theta_v$ about $\hat{e}_2^{(I)} = \hat{e}_2^{(V)}$. (*a*) The polarization vector $\vec{P}_\omega$, which describes a neutrino initially in $|\nu_e\rangle$, and its precession about $\vec{B}$. The projection of this precession motion onto the $\hat{e}_3^{(I)}$ axis represents the flavor oscillation of the neutrino. (*b*) The precession of $\vec{P}_\omega$ in the presence of ordinary matter. If the matter density varies slowly, the angle between $\vec{P}_\omega$ and $\vec{H} = \omega\vec{B} + \lambda\vec{L}$ remains constant. This represents adiabatic MSW flavor transformation of the neutrino. Also see Reference 123 for a more detailed discussion on this geometric interpretation.

ratios of $-\omega$ and $-\lambda$, respectively. (Note that a real magnetic spin **s** with the gyromagnetic ratio γ in the presence of magnetic field **B** obeys the EoM $\dot{\mathbf{s}} = -\gamma\mathbf{B} \times \mathbf{s}$.) Equivalently, $\vec{P}_\omega$ behaves as a "magnetic spin" coupled to the total "magnetic field" $\vec{H} = \omega\vec{B} + \lambda\vec{L}$ with the "gyromagnetic ratio" of -1. This picture allows geometric interpretations for both vacuum oscillations and MSW flavor transformation (**Figure 2**).

We give a few comments about the polarization vector notation before we consider neutrino self-coupling. First, the polarization vector notation is fully equivalent to the neutrino flavor isospin notation (68), where the neutrino flavor isospin for a neutrino or antineutrino is $\vec{s}_\omega = \frac{1}{2}\frac{\vec{P}_\omega}{|\vec{P}_\omega|}$. Second, in Equation 6 $\vec{P}_\omega$ is defined with a minus sign for the antineutrino. Although the physics is not changed by the choice of notation, our definition of $\vec{P}_\omega$ is convenient for analyzing collective neutrino oscillations when both neutrinos and antineutrinos are present (see Section 2.3). This notation has been adopted in the most recent literature.

2.3. Synchronized Neutrino Oscillations, Corotating Frames, and Matter Effects

The neutrino self-coupling is represented as the coupling between polarization vectors in Equation 7. Let us consider a homogeneous and isotropic neutrino gas with $\lambda = 0$ and μ constant. Use of Equation 7 shows that the so-called total energy of the "magnetic spins,"

$$\mathcal{E} = \int_{-\infty}^{\infty} \omega(\vec{P}_\omega \cdot \vec{B})\mathrm{d}\omega + \frac{\mu}{2}\vec{D}^2, \qquad 8.$$

is constant in this case (68). Here the first term is the total energy of coupling between the so-called "magnetic field" and "spins," and the second term is the total spin-spin coupling energy. If μ is large, then $|\vec{D}| \simeq \sqrt{2\mathcal{E}/\mu}$ is approximately constant. This implies that a dense neutrino

gas can experience self-maintained coherent oscillations (58). For example, if a dense neutrino gas consists initially of neutrinos of the same flavor (so that all $\vec{P}_\omega$ are initially aligned), then the flavor evolution of these neutrinos is coherent (i.e., all $\vec{P}_\omega$ remain aligned) even when they have different energies. This phenomenon has been termed synchronized neutrino oscillation because all neutrinos (and antineutrinos) in such a system oscillate collectively with (angular) frequency $\Omega_{\rm sync}$. The synchronized oscillation frequency is an average of all ωs (62):

$$\Omega_{\rm sync} = |\vec{D}|^{-2} \int_{-\infty}^{\infty} (\vec{D} \cdot \vec{P}_\omega)\omega {\rm d}\omega. \qquad 9.$$

Consider another neutrino system that is similar to the synchronized system discussed above except that the oscillation frequency ω of each neutrino or antineutrino is shifted by a common value ω_0. Any polarization vector, say $\vec{P}_\omega$, in this system should move in a way similar to $\vec{P}_{\omega-\omega_0}$ in the synchronized system, except for an extra precession about $\vec{B}$ with frequency ω_0. In other words, this system behaves just like the synchronized system in a reference frame that rotates about $\vec{B}$ with frequency ω_0. Indeed, in this noninertial corotating frame (68), each polarization vector is coupled to a nonphysical field $-\omega_0\vec{B}$, and Equation 7 (with $\lambda = 0$) becomes

$$\dot{\vec{P}}_\omega = [(\omega - \omega_0)\vec{B} + \mu\vec{D}] \times \vec{P}_\omega. \qquad 10.$$

Therefore, this neutrino system experiences synchronized flavor transformation, just like the one discussed above, but with $\Omega_{\rm sync}$ shifted by ω_0. Because the oscillation frequency ω can be shifted to any value by using an appropriate corotating frame, the criterion for synchronization should not be $\mu \gg |\langle\omega\rangle|$ but rather $\mu \gg \Delta\omega$ (68), where $\langle\omega\rangle$ and $\Delta\omega$ are the average value and the spread in ω for the neutrino system, respectively. Note that the reversal of the direction of $\vec{P}_\omega$ for the antineutrino (Equation 6) is important when the corotating frame is used. If this reversal is not incorporated into the definition of $\vec{P}_\omega$, then the direction of $\vec{P}_\omega$ also changes if the sign of the corresponding vacuum oscillation frequency changes on transformation to the corotating frame.

Note that if $\vec{B}$ is parallel to $\vec{L}$, the matter effect can be completely removed by transforming to an appropriate corotating frame. For a general case, on transforming to the corotating frame Equation 7 becomes

$$\dot{\vec{P}}_\omega = (\omega\vec{B} + \mu\vec{D}) \times \vec{P}_\omega \quad \text{and} \quad \dot{\vec{B}} = -\lambda\vec{L} \times \vec{B}. \qquad 11.$$

The matter effect does not disappear here but rather causes $\vec{B}$ to rotate in the corotating frame. If the matter density is large ($\lambda \gg |\omega|$), however, the fast-rotating $\vec{B}$ in Equation 11 can be replaced by $(\vec{B} \cdot \vec{L})\vec{L}$ for collective neutrino oscillations (68). In other words, for collective neutrino oscillations and in the presence of large matter density, matter effects may be ignored and the effective neutrino mixing parameters become $\theta_{\rm eff} \simeq 0$ and $\Delta m^2_{\rm eff} = \Delta m^2 \cos 2\theta_{\rm v}$.

2.4. Solving for Supernova Neutrino Flavor Evolution

Although collective neutrino oscillations may occur in any environment in which neutrino fluxes are significant, recent studies of this phenomenon have focused on the core-collapse supernova environment. The supernova environment is far more complex than the early universe, in part because of its inhomogeneity and anisotropy. This complexity is enhanced because neutrinos of different flavors and energies and propagating in different directions are coupled by neutrino self-interaction (50). Full simulations of neutrino oscillations with neutrino self-interaction in a general supernova environment are beyond current numerical capabilities. Here we briefly discuss two schemes commonly used in investigating collective neutrino oscillations. Both of these schemes employ the neutrino bulb model, in which the supernova environment is spherically symmetric

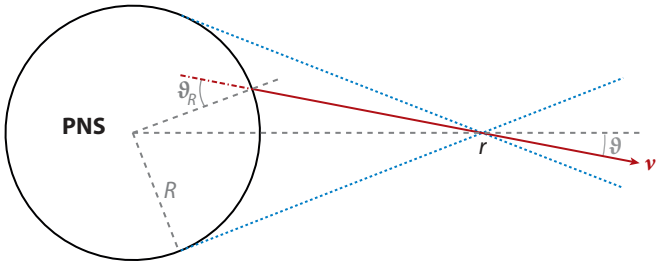

Figure 3

The geometric layout of the neutrino bulb model. In this model all neutrinos are emitted half-isotropically from the surface (neutrino sphere) of the protoneutron star (PNS), which has radius R. Spherical symmetry and isotropic emission on the neutrino sphere imply that all neutrinos with the same initial flavor, energy, and emission angle ϑ_R have identical flavor evolution histories. The neutrino polarization vector $\vec{P}_{\omega,\vartheta_R}(r)$ is uniquely determined by ω, ϑ (or ϑ_R), and r. Here ϑ is the angle at radius r between the neutrino trajectory direction and the radial direction. Figure adapted from figure 1 of Reference 70. Copyright 2006 by the American Physical Society.

around the center of the protoneutron star (PNS) (**Figure 3**). The polarization vectors in this model obey the EoM

$$\cos\vartheta \frac{\mathrm{d}}{\mathrm{d}r}\vec{P}_{\omega,\vartheta_R}(r) = [\omega\vec{B} + \lambda(r)\vec{L} + \vec{H}_{\nu\nu,\vartheta_R}(r)] \times \vec{P}_{\omega,\vartheta_R}(r), \qquad 12.$$

where

$$\vec{H}_{\nu\nu,\vartheta_R}(r) = \sqrt{2}G_{\mathrm{F}}n_{\bar{\nu}_e}(R)\int_{-\infty}^{\infty}\mathrm{d}\omega'\int_{\cos\vartheta_{\max}}^{1}\mathrm{d}(\cos\vartheta')(1-\cos\vartheta\ \cos\vartheta')\vec{P}_{\omega',\vartheta'_R}(r). \qquad 13.$$

Note that $\vartheta = \arcsin(R\sin\vartheta_R/r)$ and has the maximum value $\vartheta_{\max} = \arcsin(R/r)$ in the neutrino bulb model (**Figure 3**). Also note that here we choose to normalize $\vec{P}_\omega$ by $n_{\bar{\nu}_e}(R) = L_{\bar{\nu}_e}/(2\pi R^2\langle E_{\bar{\nu}_e}\rangle)$, the total number density of $\bar{\nu}_e$ at the neutrino sphere, where $L_{\bar{\nu}_e}$ and $\langle E_{\bar{\nu}_e}\rangle$ are the energy luminosity and the spectrum-averaged energy of $\bar{\nu}_e$ at the neutrino sphere, respectively. For the neutronization-burst epoch where the ν_e flux is much larger than the fluxes of all other neutrino species, $\vec{P}_\omega$ should be normalized by $n_{\nu_e}(R)$ instead. In typical numerical simulations, R is in the range of 10 to 60 km, and the luminosities and the average energies of neutrinos are in the ranges of 10^{50} to 10^{53} erg s^{-1} and 10 to 30 MeV, respectively.

Equation 12 can be solved numerically without any further assumptions. This is known as the multiangle scheme. The other scheme is the so-called single-angle scheme (50). In this latter scheme it is assumed that $\vec{P}_{\omega,\vartheta_R}(r) = \vec{P}_\omega(r)$ is the same for different neutrino trajectories. There are several variants of the single-angle scheme that lead to qualitatively similar results. In one of the variants, $\vec{P}_\omega(r)$ is computed along the radial direction ($\vartheta_R = 0$), and Equation 12 becomes

$$\frac{\mathrm{d}}{\mathrm{d}r}\vec{P}_\omega(r) = [\omega\vec{B} + \lambda(r)\vec{L} + \sqrt{2}G_{\mathrm{F}}n_{\bar{\nu}_e}\mathcal{D}(r/R)\vec{D}] \times \vec{P}_\omega(r), \qquad 14.$$

where the geometric factor $\mathcal{D}(r/R) = \frac{1}{2}[1-\sqrt{1-(\frac{R}{r})^2}]^2$ partially accounts for the angle effect and geometric dilution of the neutrino fluxes in the neutrino bulb model. Comparing Equations 7 and 14 shows that the flavor evolution of neutrinos in the single-angle scheme is equivalent to that of a homogeneous and isotropic neutrino gas expanding with "time" r. In this analogy, the strength of the neutrino self-coupling is $\mu(r) = \sqrt{2}G_{\mathrm{F}}n_{\bar{\nu}_e}(R)\mathcal{D}(r/R)$. The radial direction is a rather special direction in the neutrino bulb model. In another variant of the single-angle scheme, it is assumed that all neutrinos are emitted with $\vartheta_R = \pi/4$ (75). Alternatively, $\vec{H}_{\nu\nu,\vartheta}$ can be averaged over neutrino trajectories (70, 90). Each of these variants also leads to

Equation 14 when $r \gg R$. However, in this limit $\mathcal{D}(r/R) \to \frac{1}{4}\left(\frac{R}{r}\right)^4$ for these variants instead of $\frac{1}{8}\left(\frac{R}{r}\right)^4$ in the single-angle scheme that employs the radial trajectory. These variants can improve the agreement between the results of the single-angle and multiangle calculations (90). Although the single-angle scheme is frequently used for its simplicity, it must be emphasized that it misses some of the important properties (e.g., anisotropy) of the neutrino bulb model and can lead to incorrect results when such properties play important roles in collective neutrino oscillations (see Section 5).

3. SIMPLE BIPOLAR NEUTRINO SYSTEMS

3.1. Bipolar Systems and the Flavor Pendulum

To illustrate another important example of collective neutrino oscillations, let us consider a homogeneous and isotropic gas that initially consists of monoenergetic ν_e and $\bar{\nu}_e$. This neutrino system is represented by two polarization vectors, $\vec{P}_\omega$ and $\vec{P}_{-\omega}$, for the neutrino and the antineutrino, respectively. We assume that $\lambda = 0$, that μ is fixed, and that $|\vec{P}_\omega| = (1+\varepsilon)|\vec{P}_{-\omega}|$, where ε is the fractional excess of neutrinos over antineutrinos. At $t = 0$, $\vec{P}_\omega$ points in the direction of $\hat{e}_3^{(\mathrm{I})}$, which is tilted away from $\hat{e}_3^{(\mathrm{V})}$ by $2\theta_\mathrm{v}$, and $\vec{P}_{-\omega}$ points in the direction opposite to $\vec{P}_\omega$. Neutrino systems that are represented by two nearly oppositely directed polarization vector groups are termed bipolar systems. Using the corotating frame technique, the discussion in this section easily can be applied to, for instance, a gas consisting initially of ν_e and ν_μ with energies $E_{\nu_e} \neq E_{\nu_\mu}$.

A peculiar case is one in which $\varepsilon = 0$ and $\vec{P}_\omega$ is initially aligned with $\hat{e}_3^{(\mathrm{V})} = -\vec{B}$ (i.e., $\theta_\mathrm{v} = 0$). On the one hand, use of energy conservation (Equation 8) demonstrates (68) that if $\omega > 0$, neither $\vec{P}_\omega$ nor $\vec{P}_{-\omega}$ can move, and so the initial configuration of the system is absolutely stable. On the other hand, if $\omega < 0$ and $\mu \gg |\omega|$, $\vec{P}_\omega$ and $\vec{P}_{-\omega}$ can nearly swap their directions (but with a slight bend toward each other). This implies that the initial configuration of the system is unstable. Therefore, the $\nu_e - \bar{\nu}_e$ system may experience insignificant flavor oscillations when $\Delta m^2 > 0$ and $\theta_\mathrm{v} \ll 1$. However, this system can experience significant flavor oscillations when $\Delta m^2 < 0$ and $\theta_\mathrm{v} \ll 1$. Such collective neutrino oscillations are known as bipolar oscillations.

The EoMs of the simple bipolar system,

$$\dot{\vec{P}}_\omega = (\omega\vec{B} + \mu\vec{D}) \times \vec{P}_\omega, \quad \text{and} \quad \dot{\vec{P}}_{-\omega} = (-\omega\vec{B} + \mu\vec{D}) \times \vec{P}_{-\omega}, \tag{15.}$$

have been solved analytically (58, 59). Instead of presenting this solution, let us rewrite Equation 15 as (71)

$$\dot{\vec{D}} = \mu^{-1}\vec{q} \times \vec{g} \quad \text{and} \quad \vec{D} = \mu^{-1}\vec{q} \times \dot{\vec{q}} + \sigma_\mathrm{s}\vec{q}, \tag{16.}$$

where $\vec{q} = \vec{Q}/|\vec{Q}| = (\vec{P}_\omega - \vec{P}_{-\omega} - \frac{\omega}{\mu}\vec{B})/|\vec{Q}|$, $\vec{g} = -\mu\omega|\vec{Q}|\vec{B}$, and $\sigma_\mathrm{s} = \vec{q} \cdot \vec{D}$ is constant. Equation 16 describes the motion of a fictitious gyroscopic pendulum, or flavor pendulum, with total angular momentum $\vec{D}$ in a uniform gravitational field in which the acceleration of gravity is $\vec{g}$. The pendulum consists of a massless rod with a point particle of mass μ^{-1} and spin σ_s attached to the end of the rod at position $\vec{q}$. The flavor pendulum that represents a symmetric bipolar system ($\varepsilon = 0$) has no internal spin. The stable and unstable configurations of the system discussed above correspond to the lowest and highest positions, respectively, that the pendulum can reach.

Generally, the flavor pendulum can experience two kinds of motion: a precession about the $\vec{B}$ axis and a nutation around the average precession track. The nutation motion corresponds to bipolar neutrino oscillations. However, like a child's top, the flavor pendulum can "defy gravity" and precess almost uniformly if μ is large enough. Specifically, the flavor pendulum can become

a so-called sleeping top and does not fall from its highest position if (71, 73)

$$\mu > \mu_{\rm cr} \equiv \frac{2|\omega|}{(\sqrt{1+\varepsilon}-1)^2}. \qquad 17.$$

This precession behavior of the flavor pendulum in the large μ limit represents synchronized oscillations of the bipolar system with $\Omega_{\rm sync} = (1 + 2\varepsilon^{-1})\omega$.

3.2. Bipolar Systems with Slowly Decreasing Neutrino Density

Let us now focus on the IH case with $\theta_{\rm v} \ll 1$. Significant neutrino oscillations can occur in this case. If the neutrino density decreases, the mass μ^{-1} of the pendulum becomes larger. The swing amplitude of the pendulum that represents a symmetric bipolar system decreases as μ decreases. The maximum swing amplitude of this pendulum can be found in the adiabatic limit where μ changes slowly (73). In this case, $\vec{P}_\omega$ and $\vec{P}_{-\omega}$ become aligned and antialigned, respectively, with $\vec{B}$ (i.e., $\nu_e \to \nu_2$ and $\bar{\nu}_e \to \bar{\nu}_2$) as μ decreases toward 0.

The asymmetric bipolar system is more interesting. Neutrino oscillations in this case are synchronized, and the flavor pendulum precesses uniformly in the limit $\mu \gg |\omega|$. If μ decreases very slowly, the flavor pendulum can still experience a nearly pure precession motion for any given μ. In this case, $\vec{P}_\omega$ and $\vec{P}_{-\omega}$ lie in the same plane with $\vec{B}$, and their directions can be readily solved for (**Figure 4**) (73, 79). Assuming $\varepsilon > 0$, $\vec{P}_{-\omega}$ becomes antialigned with $\vec{B}$ (i.e., $\bar{\nu}_e \to \bar{\nu}_2$) as $\mu \to 0$. Meanwhile the direction of $\vec{P}_\omega$ can be determined from the constancy of $\vec{D} \cdot \vec{B}$ (71; also see Equation 16, where $\vec{g} \propto \vec{B}$).

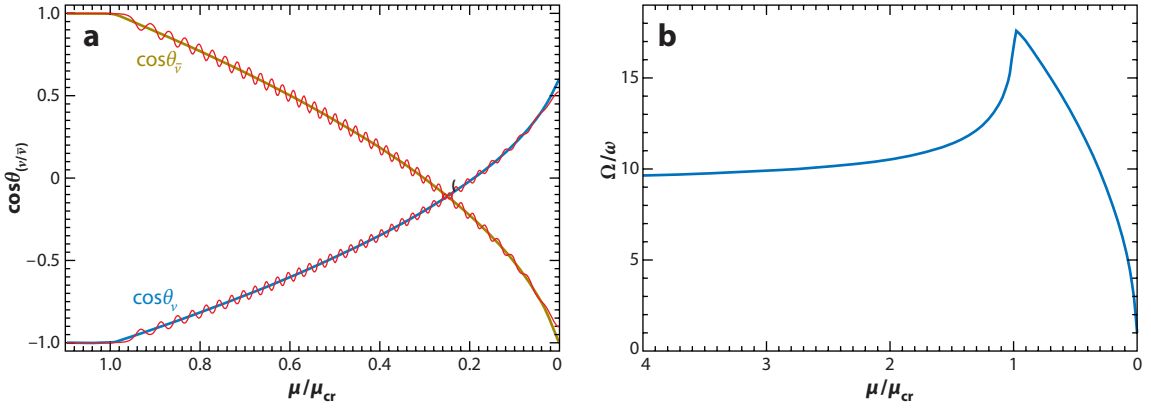

Figure 4

Evolution with decreasing μ for a simple bipolar system that consists initially of monoenergetic ν_e and $\bar{\nu}_e$. The neutrino excess is $\varepsilon = 0.25$, and the mixing parameters are $\theta_{\rm v} = 0.01$ and $\Delta m^2 < 0$. (*a*) The configuration of the polarization vectors, where θ_ν ($\theta_{\bar{\nu}}$) is the angle between $\vec{P}_\omega$ ($\vec{P}_{-\omega}$) and $\vec{B} = -\hat{e}_3^{(\rm V)}$. The thick colored lines represent an assumed pure precession motion for the flavor pendulum, and the thin wavy red lines represent a case where μ decreases slowly and linearly with time. At $\mu \gtrsim \mu_{\rm cr}$ the flavor pendulum is a so-called sleeping top, and there are no flavor oscillations. When $\mu < \mu_{\rm cr}$, the flavor pendulum experiences precession as well as nutation around the average precession track. (*b*) The precession frequency Ω of the flavor pendulum, assuming that it is executing pure precession. In this case, the value Ω approaches $\Omega_{\rm sync}$ and ω in the limits $\mu \to \infty$ and $\mu \to 0$, respectively. The analytical solution for the pure precession motion of the polarization vectors can be found in Reference 79. This figure is adapted from figures 3*a* and 4 in Reference 73. Copyright 2007 by the American Physical Society.

4. ISOTROPIC AND HOMOGENEOUS NEUTRINO GASES

4.1. Static Solutions for the Neutrino Flavor Evolution Equation

Here we consider a homogeneous and isotropic gas that consists of neutrinos with continuous energy spectra. Let us first seek static solutions to the EoM for the polarization vectors (Equation 7) for the case in which both the matter density and the neutrino densities are constant. One possibility is that the solution is stationary and that the $\vec{P}_\omega$s do not evolve with time t. This solution is only possible if the "spin" $\vec{P}_\omega$ is parallel to the corresponding total "magnetic field" $\vec{H}_\omega = \omega\vec{B} + \lambda\vec{L} + \mu\vec{D}$. For this case, and noting that $\vec{H}_\omega$ does not depend on $\vec{P}_\omega$, we can obtain the following equations for the total polarization vector $\vec{D}$ (76):

$$D_1 = (\lambda \sin 2\theta_v + \mu D_1)\int_{-\infty}^{\infty} \frac{\epsilon_\omega |\vec{P}_\omega|}{|\vec{H}_\omega|} d\omega, \qquad 18a.$$

$$D_2 = \mu D_2 \int_{-\infty}^{\infty} \frac{\epsilon_\omega |\vec{P}_\omega|}{|\vec{H}_\omega|} d\omega, \qquad 18b.$$

and

$$D_3 = \int_{-\infty}^{\infty} (-\omega + \lambda \cos 2\theta_v + \mu D_3)\frac{\epsilon_\omega |\vec{P}_\omega|}{|\vec{H}_\omega|} d\omega, \qquad 18c.$$

where $D_a = \vec{D}\cdot\hat{e}_a^{(V)}$ ($a = 1, 2, 3$) and $\epsilon_\omega = +1$ (-1) if $\vec{P}_\omega$ is aligned (antialigned) with $\vec{H}_\omega$. The stationary solution to the EoM for $\vec{P}_\omega$ can be found from Equations 18*a–c* and the alignment condition. We note that Equations 18*a* and 18*b* generally imply that $D_2 = 0$ if $\lambda \neq 0$, which in turn implies that $\vec{P}_\omega \cdot \hat{e}_2^{(V)} = 0$ for any ω.

Equations 18*a* and 18*b* become equivalent when $\lambda = 0$, and $\vec{D}$ is underconstrained by Equations 18*a–c* in this case because when $\lambda = 0$, the EoM for $\vec{P}_\omega$ possesses a rotational symmetry about $\vec{B}$. In other words, if $\{\vec{P}_\omega(t)|\forall\omega\}$ (meaning the polarization vectors for all frequencies ω at a given time t) solves the EoM, then $\{\vec{P}'_\omega(t)|\forall\omega\}$ also solves the EoM, in which $\vec{P}'_\omega(t)$ is obtained from $\vec{P}_\omega(t)$ by rotation about $\vec{B}$ by an arbitrary angle ϕ. Here ϕ is independent of ω and t. This is a generalization of the rotational symmetry of the flavor pendulum about the "gravity" vector $\vec{g} \propto \vec{B}$. Such a continuous symmetry in the EoMs generally implies the existence of collective motion and a conservation law. For example, a translational symmetry of a group of particles along some direction implies the possibility of the collective motion of the particles in that direction and the conservation of the total momentum of the particles in the same direction. As discussed in Section 3, for the simple bipolar system this rotational symmetry implies the possibility of a pure precession of the flavor pendulum in which both polarization vectors of the system precess with the same frequency Ω. Therefore, it is natural to seek a static solution to the EoM in which $\lambda = 0$, and μ is a constant, and all the $\vec{P}_\omega$s precess about $\vec{B}$ with the same frequency Ω. In this case, all the $\vec{P}_\omega$s are stationary in a corotating frame, which rotates about $\vec{B}$ with frequency Ω. In this corotating frame, $\vec{P}_\omega$ is either aligned or antialigned with $\tilde{\vec{H}}_\omega = (\omega - \Omega)\vec{B} + \mu\vec{D}$, and the components of $\vec{D}$ in the corotating frame can be found from equations similar to Equations 18*a–c*. These equations can be recast as the following two simple sum rules (74):

$$1 = \int_{-\infty}^{\infty} \frac{\epsilon_\omega |\vec{P}_\omega|}{\sqrt{[(\Omega - \omega)/\mu + D_3]^2 + D_\perp^2}} d\omega \qquad 19.$$

and

$$\Omega = \int_{-\infty}^{\infty} \frac{\epsilon_\omega \omega |\vec{P}_\omega|}{\sqrt{[(\Omega - \omega)/\mu + D_3]^2 + D_\perp^2}} d\omega, \qquad 20.$$

where $D_\perp$ is the component of $\vec{D}$ that is perpendicular to $\hat{e}_3^{(V)}$. The rotational symmetry of the system about $\vec{B}$ implies that $D_3 = -\vec{D} \cdot \vec{B}$ is constant.

4.2. Adiabatic Solutions and the Spectral Swap/Split

If λ and μ vary slowly with time, adiabatic solutions that correspond to the static solutions discussed above can be obtained. We term them the (adiabatic, ν-enhanced) MSW solution and the (adiabatic) precession solution. **Figure 5** shows these two adiabatic solutions for a single-angle scheme, together with the corresponding numerical solutions for Equation 14. In these calculations it is assumed that (*a*) the most abundant neutrino species at the neutrino sphere are ν_e and $\bar{\nu}_e$ and (*b*) $\theta_v \ll 1$. For the precession solution the matter field is removed with an appropriate corotating frame. The flavor pendulum model provides insight into how the numerical solution evolves from the MSW solution toward the precession solution. In the IH case, a large matter density essentially keeps the flavor pendulum (with $\varepsilon > 0$) near its highest position. This configuration becomes unstable when $\mu < \mu_{cr}$. In the NH case, the ν-enhanced MSW flavor transformation raises the flavor pendulum to near its highest position, and the configuration again becomes unstable when $\mu < \mu_{cr}$.

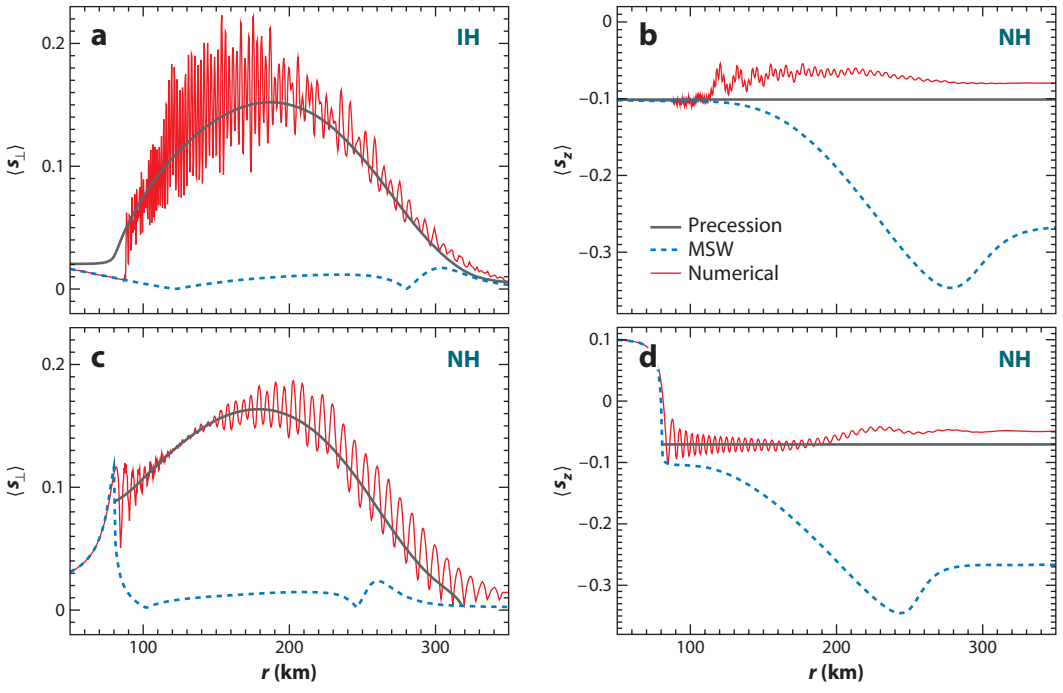

Figure 5

Comparison of the numerical solution, the ν-enhanced Mikheyev-Smirnov-Wolfenstein (MSW) solution, and the precession solution in a single-angle scheme, where $\theta_v = 0.1$, $\langle s_\perp \rangle \propto D_\perp$, and $\langle s_z \rangle \propto D_3$. The numerical solution initially follows the MSW solution. (*a*) In the inverted neutrino mass hierarchy (IH) case, the MSW solution becomes unstable at $r \simeq 88$ km, and thereafter the numerical solution shows oscillations around the precession solution. (*b*) In the normal neutrino mass hierarchy (NH) case, the numerical solution follows the MSW solution through the resonance (where $\langle s_z \rangle \simeq 0$) before it shifts to follow the precession solution track. Figure adapted from figure 1 of Reference 76. Copyright 2007 by the American Physical Society.

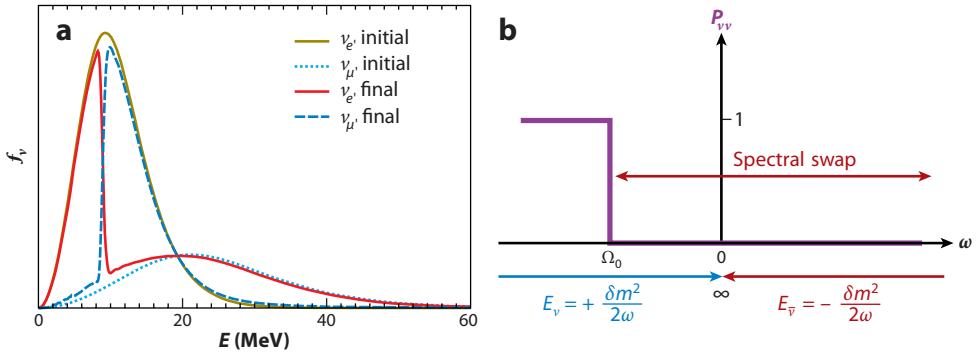

Figure 6

Illustration of the stepwise spectral swap phenomenon in the two-flavor mixing case with $\Delta m^2 < 0$ (inverted neutrino mass hierarchy) that was discovered by Duan et al. (70). (*a*) The stepwise swapping of ν_e and ν_μ energy spectra about $E_s \simeq 9$ MeV in a single-angle scheme. The spectra of $\bar\nu_e$ and $\bar\nu_\mu$ are nearly fully swapped in this calculation. (*b*) The corresponding survival probability $P_{\nu\nu}$, which is a step-like function of ω. For the normal neutrino mass hierarchy case, the step-like structure of $P_{\nu\nu}(\omega)$ is pushed rightward to $\Omega_0 > 0$. Because $E_s = |\frac{\Delta m^2}{2\Omega_0}|$ splits a neutrino spectrum into two parts with different flavors, this phenomenon is also sometimes termed spectral split. Reprinted with permission from Reference 124. Copyright 2009, American Institute of Physics.

Just as in the conventional adiabatic MSW flavor transformation case (**Figure 2**), in the adiabatic precession solution $\vec{P}_\omega$ follows $\vec{H}_\omega$, whose direction (and magnitude) changes as μ decreases. This induces neutrino flavor transformation. Specifically, as $\mu \to 0$, $\vec{H}_\omega \to (\omega - \Omega_0)\vec{B}$, where $\Omega_0 = \Omega(\mu = 0)$. This means that the adiabatic collective precession mode converts the initial ν_e into the mass state $|\nu_1\rangle$ or $|\nu_2\rangle$, depending on whether ω is smaller or larger than Ω_0 (70). This phenomenon, known as the stepwise spectral swap or spectral split, is most dramatic when $\theta_v \ll 1$ (**Figure 6**). The swap/split energy $E_s = |\frac{\Delta m^2}{2\Omega_0}|$ can be determined from the constancy of $\vec{D} \cdot \vec{B}$ (74).

4.3. Precession Solution in the Three-Flavor Mixing Scenario

The neutrino polarization vector defined in Equation 6 can be easily generalized to the three-flavor mixing scenario by replacing the Pauli matrices with the Gell-Mann matrices Λ_a ($a = 1, 2, \ldots, 8$) (83, 123). However, because an eight-dimensional polarization vector, or Bloch vector, cannot be as easily visualized as its three-dimensional counterpart, we discuss the collective precession mode by using the matrix formalism. To this end, we define the polarization matrix $\mathsf{P}_\omega = \frac{1}{2}\sum_{a=1}^{8}(P_{\omega,a}\Lambda_a)$, where $P_{\omega,a}$ is the ath component of the Bloch vector $\vec{P}_\omega$. We note that here the definition of the Bloch vector $\vec{P}_\omega$ follows the same sign convention for antineutrinos as in Equation 6. The polarization matrix obeys the EoM

$$i\dot{\mathsf{P}}_\omega = [\omega_L \mathsf{B}_L + \omega_H \mathsf{B}_H + \mu \mathsf{D}, \mathsf{P}_\omega], \qquad 21.$$

where $\mathsf{D} = \int_{-\infty}^{\infty} \mathsf{P}_\omega d\omega$ is the total polarization matrix. In Equation 21, $\omega_L = \pm\frac{\delta m^2}{2E}$ and $\mathsf{B}_L = -\frac{1}{2}\Lambda_3$ (in the mass basis) correspond to the small mass splitting, which we define as $\delta m^2 \equiv m_2^2 - m_1^2 \simeq \Delta m^2_\odot$. Also in Equation 21, $\omega_H = \omega = \pm\frac{\Delta m^2}{2E}$ and $\mathsf{B}_H = -\frac{1}{\sqrt{3}}\Lambda_8$ (in the mass basis) correspond to the large mass splitting, which we define as $\Delta m^2 = m_3^2 - \frac{1}{2}(m_1^2 + m_2^2) \simeq \pm\Delta m^2_{atm}$. For simplicity

we have ignored the matter field because it can be removed by employing the corotating frame technique (84).

The static precession solution (with constant μ) can be obtained by assuming that $\{\tilde{\mathsf{P}}_\omega, \Omega_\mathrm{L}, \Omega_\mathrm{H} \mid \forall\omega\}$ solves the equation

$$[\tilde{\mathsf{H}}_\omega, \tilde{\mathsf{P}}_\omega] = [(\omega_\mathrm{L} - \Omega_\mathrm{L})\mathsf{B}_\mathrm{L} + (\omega_\mathrm{H} - \Omega_\mathrm{H})\mathsf{B}_\mathrm{H} + \mu\tilde{\mathsf{D}}, \tilde{\mathsf{P}}_\omega] = 0, \quad 22.$$

where $\tilde{\mathsf{P}}_\omega$, Ω_L, and Ω_H are constant and $\tilde{\mathsf{D}} = \int_{-\infty}^{\infty} \tilde{\mathsf{P}}_\omega \, \mathrm{d}\omega$. In the two-flavor mixing scenario ($\mathsf{B}_\mathrm{L} = 0$), Equation 22 corresponds to the condition that the "spin" $\vec{\tilde{P}}_\omega$ is stationary in a corotating frame and parallel to the total "magnetic field" $\vec{\tilde{H}}_\omega$ in this reference frame. Equation 22 is known as the precession ansatz (84) because it implies a static precession solution to the EoM (Equation 21). This solution, $\{\mathsf{P}_\omega(t), \Omega_\mathrm{L}, \Omega_\mathrm{H} \mid \forall\omega\}$, can be written as

$$\mathsf{P}_\omega(t) = \exp[-\mathrm{i}(\Omega_\mathrm{L}\mathsf{B}_\mathrm{L} + \Omega_\mathrm{H}\mathsf{B}_\mathrm{H})t]\tilde{\mathsf{P}}_\omega \exp[\mathrm{i}(\Omega_\mathrm{L}\mathsf{B}_\mathrm{L} + \Omega_\mathrm{H}\mathsf{B}_\mathrm{H})t]. \quad 23.$$

Because $\tilde{\mathsf{P}}_\omega$ and $\tilde{\mathsf{H}}_\omega$ commute, they can be simultaneously diagonalized by a unitary matrix X. Therefore, we have $\mathsf{X}\tilde{\mathsf{H}}_\omega\mathsf{X}^\dagger = \mathrm{diag}[\tilde{h}_{\omega,1}, \tilde{h}_{\omega,2}, \tilde{h}_{\omega,3}]$, where $\tilde{h}_{\omega,1} < \tilde{h}_{\omega,2} < \tilde{h}_{\omega,3}$, and $\mathsf{X}\tilde{\mathsf{P}}_\omega\mathsf{X}^\dagger = \mathrm{diag}[\tilde{p}_{\omega,1}, \tilde{p}_{\omega,2}, -(\tilde{p}_{\omega,1} + \tilde{p}_{\omega,2})]$. When μ varies slowly with t, the adiabatic precession solution can be obtained from the static precession solutions (with different μ) by using the adiabatic ansatz (84)

$$\frac{\partial}{\partial\mu}\tilde{p}_{\omega,1} = \frac{\partial}{\partial\mu}\tilde{p}_{\omega,2} = 0. \quad 24.$$

In the two-flavor mixing scenario, the adiabatic ansatz corresponds to the assumption that $\vec{P}_\omega$ remains parallel to $\vec{\tilde{H}}_\omega$. If neutrinos follow the adiabatic precession solution, then as $\mu \to 0$, $\tilde{\mathsf{P}}_\omega$ becomes a diagonal matrix in the mass basis (see Equation 22). The diagonal elements of $\mathsf{P}_\omega|_{\mu=0} = \tilde{\mathsf{P}}_\omega|_{\mu=0}$ are $\tilde{p}_{\omega,1}$, $\tilde{p}_{\omega,2}$, and $-(\tilde{p}_{\omega,1} + \tilde{p}_{\omega,2})$, and these elements have the same order of appearance as the diagonal elements of $\mathsf{H}_\omega|_{\mu=0} = (\omega_\mathrm{L} - \Omega_\mathrm{L})\mathsf{B}_\mathrm{L} + (\omega_\mathrm{H} - \Omega_\mathrm{H})\mathsf{B}_\mathrm{H}$. For example, in the mass basis we have $\mathsf{P}_\omega|_{\mu=0} = \mathrm{diag}[\tilde{p}_{\omega,2}, \tilde{p}_{\omega,1}, -(\tilde{p}_{\omega,1} + \tilde{p}_{\omega,2})]$ if $\tilde{\mathsf{H}}_\omega|_{\mu=0} = \mathrm{diag}[\tilde{h}_{\omega,2}, \tilde{h}_{\omega,1}, \tilde{h}_{\omega,3}]$, where $\tilde{h}_{\omega,1} < \tilde{h}_{\omega,2} < \tilde{h}_{\omega,3}$. The fact that $\mathsf{P}_\omega|_{\mu=0}$ is diagonal in the mass basis implies that there can be multiple spectral swaps/splits in the final neutrino energy spectra. Because $\alpha = \frac{\delta m^2}{|\Delta m^2|} \ll 1$, these spectral swaps/splits form hierarchically and appear at different neutrino densities (**Figure 7**).

5. ANISOTROPIC AND/OR INHOMOGENEOUS NEUTRINO GASES

5.1. Kinematic Decoherence of Collective Neutrino Oscillations

The oscillations of neutrinos with different momenta can become out of phase (i.e., collective oscillations can break down), which is sometimes referred to as kinematic decoherence. Of course, this is not to be confused with quantum decoherence, which can be induced by any neutrino scattering process that changes neutrino momentum. In a homogeneous and isotropic neutrino gas, the condition for kinematic decoherence is $\Delta\omega \gg \mu$. In this limit, the coupling among "spins" is not strong enough to maintain a collective motion, and $\vec{P}_\omega$ precesses about $\vec{B}$ with vacuum oscillation frequency ω. In Section 2.3 we showed that, when $\Delta\omega \ll \mu$, synchronized neutrino oscillations do not decohere kinematically, and $|\vec{D}|$ is approximately constant because of energy conservation. Numerical simulations suggest that bipolar neutrino oscillations are also stable (55, 57), although as yet we know of no conservation law that could explain this phenomenon.

If collective neutrino oscillations also exist in an anisotropic environment, then the wave fronts of the oscillation waves of the neutrinos must coincide with one another. In the neutrino bulb

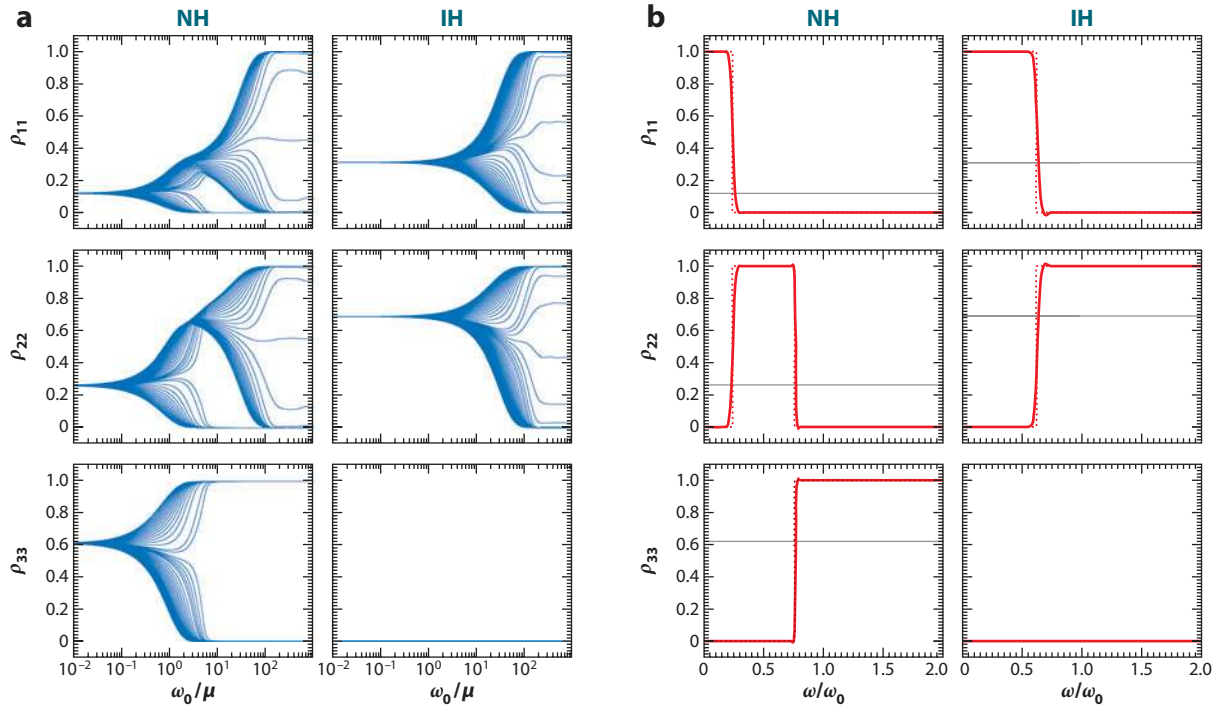

Figure 7

The evolution of the diagonal elements of the neutrino density matrices in the mass basis during the hierarchical formation of spectral swaps/splits in a neutrino gas. Initially P_ω, and the density matrix ρ_ω, is the same across the whole energy spectrum $\omega \in [0, 2\omega_0]$ (*a*, *thin blue lines*). When $\mu \gg \omega_0$, all neutrinos are in the heaviest eigenstate (i.e., the state with the largest eigenvalue) of $\tilde{\mathsf{H}}_\omega \simeq \mu\tilde{\mathsf{D}}$. For the normal neutrino mass hierarchy (NH) case, two spectral swaps/splits form hierarchically at $\mu \sim \omega_0$ and $\mu \sim \alpha\omega_0$, respectively. Curves in panel *a* give ρ_ω with various values of ω. At $\omega_0 \gg \mu \gg \alpha\omega_0$, the heaviest eigenstate of $\tilde{\mathsf{H}} \simeq (\omega - \Omega_{\mathrm{H},0})\mathsf{B}_\mathrm{H} + \mu\tilde{\mathsf{D}}$ is $|\nu_3\rangle$ for neutrinos with $\omega > \Omega_{\mathrm{H},0}$. Subsequently these neutrinos no longer participate in collective oscillations. At $\mu \ll \alpha\omega_0$, the remaining neutrinos are in $|\nu_2\rangle$ or $|\nu_1\rangle$, depending on whether $\omega_\mathrm{L} = \alpha\omega$ is larger or smaller than $\Omega_{\mathrm{L},0}$. In either case, the state corresponds to the heaviest eigenstate of $\tilde{\mathsf{H}}_\omega \simeq (\omega_\mathrm{L} - \Omega_{\mathrm{L},0})\mathsf{B}_\mathrm{L}$ (ignoring the decoupled state $|\nu_3\rangle$). This leads to two spectral swaps/splits in the final neutrino energy spectra (*b*, *thick red lines in the NH column*). In the inverted neutrino mass hierarchy (IH) case, the ρ_{33} are initially set to zero for all ω. As a result, $|\nu_3\rangle$ is completely decoupled from the equation of motion, and no spectral swap/split forms at $\mu \sim \omega_0$. The dotted red lines in panel *b* are computed by using the constancy of $\mathrm{Tr}(\mathsf{D} \cdot \Lambda_3)$ and $\mathrm{Tr}(\mathsf{D} \cdot \Lambda_8)$ and by assuming that the spectral swaps/splits are infinitely sharp. Figure reprinted with permission from Reference 85. Copyright 2008 by the American Physical Society.

model these wave fronts are spheres that cocenter with the PNS. However, in this model a neutrino propagating along a nonradial trajectory would travel a longer distance than would a radially propagating neutrino (50). In other words, a nonradially propagating neutrino appears to have a larger oscillation frequency $\omega' = \omega/\cos\vartheta$ along r (see Equation 12). This frequency would enlarge $\Delta\omega$ and would require stronger neutrino self-coupling to maintain collective oscillations among neutrinos propagating along different trajectories. Note that the "magnetic field" $\vec{H}_{\nu\nu,\vartheta}(r)$ generated by other "spins" is trajectory dependent, which adds another potential source of kinematic decoherence.

Raffelt & Sigl (72) pointed out that a neutrino gas with an initially symmetric bipolar configuration (i.e., $\vec{P}_\nu = -\vec{P}_{\bar{\nu}}$) can experience quick kinematic decoherence even in the presence of a small anisotropy, and in this case, both $|\vec{P}_\nu|$ and $|\vec{P}_{\bar{\nu}}|$ evolve toward zero. Later it was found that an asymmetric bipolar neutrino system [i.e., $|\vec{P}_\nu| = (1+\varepsilon)|\vec{P}_{\bar{\nu}}|$ with $\varepsilon \neq 0$] may or may not experience

kinematic decoherence, depending on the value of ε (75). For typical choices of other parameters in a neutrino bulb model, kinematic decoherence is suppressed if $\varepsilon \gtrsim 0.3$.

In the above discussion, we have ignored ordinary matter. In the presence of a large matter density, $\vec{P}_\omega$ tends to precess around $-\vec{L}$ with frequency $\omega' = -\lambda + \omega \cos 2\theta_v$. In the isotropic environment, $\omega' \to \omega \cos 2\theta_v$ in the corotating frame that rotates about $\vec{L}$ with frequency λ. In this case, therefore, when neutrinos experience collective oscillations, ordinary matter can be ignored. In an anisotropic environment, such as the neutrino bulb model, we have a frequency of $\omega' = (-\lambda + \omega \cos 2\theta_v)/\cos\vartheta$ along r. Clearly, it is not possible to remove the matter effect for all neutrino trajectories, which implies that collective neutrino oscillations would not exist in a region where the net number density of electrons is much larger than that of neutrinos (91).

5.2. Precession Mode in the Anisotropic Environment

In Section 3 we showed that with $\varepsilon \neq 0$ the flavor pendulum possesses an internal spin. The existence of this internal spin makes it possible for the flavor pendulum to experience a precession motion and a nutation motion simultaneously. These two kinds of motion of the flavor pendulum correspond to the precession mode and the bipolar mode of neutrino oscillations. The findings in References 72 and 75 suggest that bipolar neutrino oscillations, which are the most prominent when ε is small, become noncollective in the anisotropic environment. These findings also suggest that the precession mode, which becomes important for cases with sufficiently large ε, can remain collective in the anisotropic environment. This hypothesis is partially supported by the fact that neutrino oscillations calculated in the single-angle scheme and in the multiangle scheme possess common features, such as the spectral swap/split phenomenon, which—as explained with the single-angle supernova scheme or in homogeneous and isotropic environments—results from neutrino oscillations in the collective precession mode.

The EoM of the polarization vectors in a stationary environment can be written as (114, 116, 125)

$$\hat{\mathbf{p}} \cdot \nabla \vec{P}_{\omega,\hat{\mathbf{p}}}(\mathbf{x}) = [\omega \vec{B} + \vec{H}_{\nu\nu,\hat{\mathbf{p}}}(\mathbf{x})] \times \vec{P}_{\omega,\hat{\mathbf{p}}}(\mathbf{x}), \qquad 25.$$

where $\lambda = 0$ for now, all the polarization vectors are normalized by $n_\nu(\mathbf{x}_0)$, the number density of neutrino species ν at location $\mathbf{x}_0$, and

$$\vec{H}_{\nu\nu,\hat{\mathbf{p}}}(x) = \sqrt{2} G_F n_\nu(\mathbf{x}_0) \int_{-\infty}^{\infty} d\omega' \int d^2\hat{\mathbf{p}}'(1 - \hat{\mathbf{p}} \cdot \hat{\mathbf{p}}') \vec{P}_{\omega',\hat{\mathbf{p}}'}(\mathbf{x}). \qquad 26.$$

As in the isotropic neutrino gas case, Equation 25 also exhibits rotational symmetry about $\vec{B}$. If $\{\vec{P}_{\omega,\hat{\mathbf{p}}}(\mathbf{x}) \,|\, \forall \omega, \hat{\mathbf{p}}\}$ solves the EoM, then $\{\vec{P}'_{\omega,\hat{\mathbf{p}}}(\mathbf{x}) \,|\, \forall \omega, \hat{\mathbf{p}}\}$ also solves the EoM; in the latter, $\vec{P}'_{\omega,\hat{\mathbf{p}}}(\mathbf{x})$ is obtained from $\vec{P}_{\omega,\hat{\mathbf{p}}}(\mathbf{x})$ by rotation about $\vec{B}$ by an arbitrary angle ϕ, and ϕ is independent of ω, $\hat{\mathbf{p}}$, and $\mathbf{x}$. This symmetry leads to the conservation law (93)

$$\nabla \cdot \left[\int_{-\infty}^{\infty} d\omega \int d^2\hat{\mathbf{p}} (\vec{P}_{\omega,\hat{\mathbf{p}}} \cdot \vec{B}) \hat{\mathbf{p}} \right] = 0. \qquad 27.$$

The rotational symmetry of the EoM about $\vec{B}$ can lead to a collective precession mode for neutrino oscillations (**Figure 8**), even in an anisotropic environment.

Let $\mathbf{K}$ be the wave vector of the collective neutrino oscillation wave in a stationary environment. If $\vec{P}_{\omega,\hat{\mathbf{p}}}$ experiences pure precession, then this vector must precess about $\vec{B}$ with frequency $\hat{\mathbf{p}} \cdot \mathbf{K}$ (in flavor space) as the corresponding neutrino propagates along its world line (in coordinate space). Similar to the isotropic neutrino gas case, this means that $\vec{P}_{\omega,\hat{\mathbf{p}}}$ is parallel to $\vec{\tilde{H}}_{\omega,\hat{\mathbf{p}}} = (\omega - \hat{\mathbf{p}} \cdot \mathbf{K})\vec{B} + \vec{H}_{\nu\nu,\hat{\mathbf{p}}}$. Therefore the corresponding neutrino or antineutrino must be in a mass

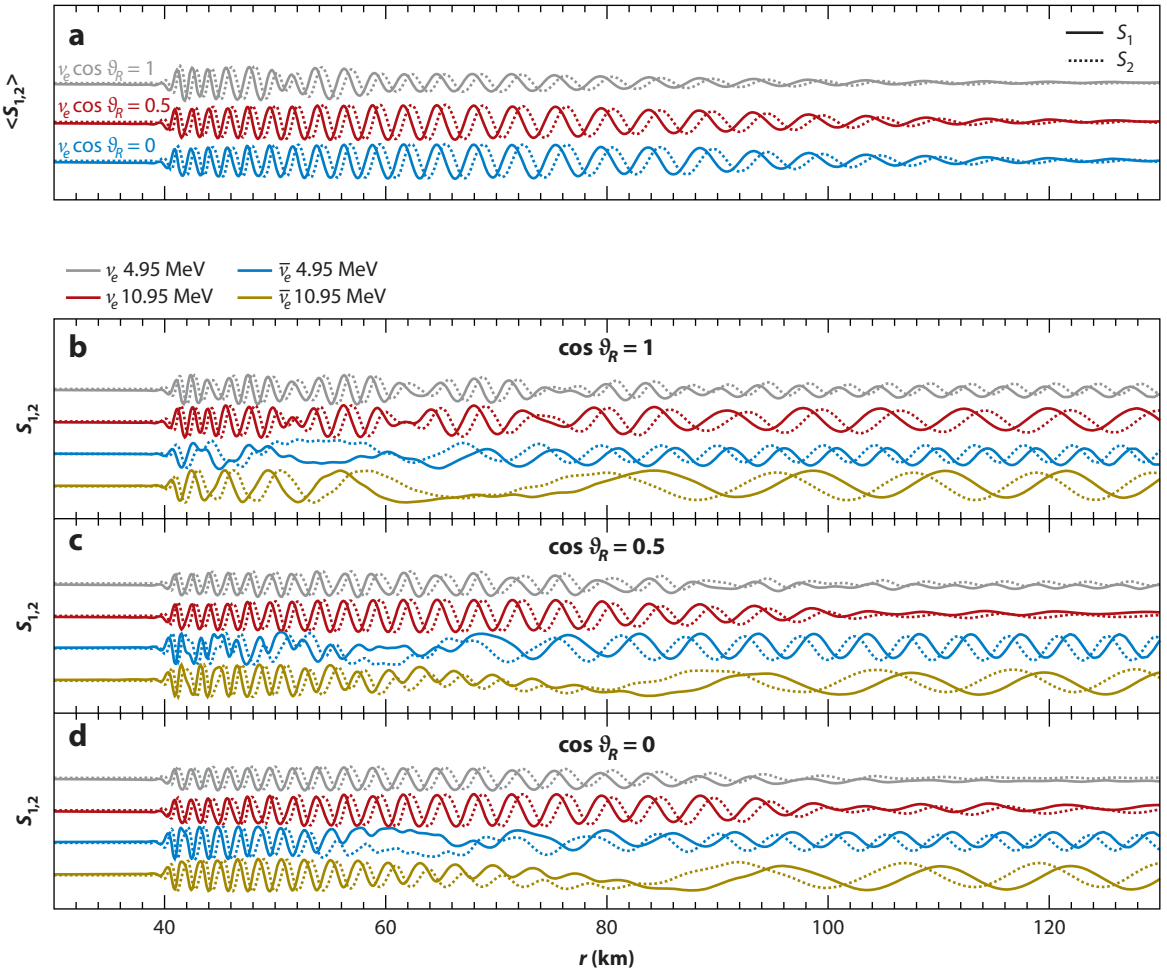

Figure 8

The collective precession of $\vec{P}_{\omega,\vartheta_R}$ in a neutrino bulb model with $\theta_v \ll 1$ and the inverted mass hierarchy ($\Delta m^2 < 0$). (*b–d*) For most neutrinos the "spin components" $s_1 \propto \vec{P}_{\omega,\vartheta_R} \cdot \hat{e}_1^{(V)}$ and $s_2 \propto \vec{P}_{\omega,\vartheta_R} \cdot \hat{e}_2^{(V)}$ oscillate in phase right after collective neutrino oscillations begin (for this case, at $r \simeq 40$ km). In-phase oscillations of s_1 and s_2 and the constant relative phase of these components imply the collective precession of the polarization vectors. The neutrinos or antineutrinos that drop out of the collective precession mode at smaller radii are those with vacuum oscillation frequencies that are farther from the collective oscillation frequency and those propagating along trajectories with larger $\cos \vartheta_R$. (*a*) The energy-averaged components $\langle s_1 \rangle$ and $\langle s_2 \rangle$. The collective precession mode stands out when noncollective neutrino oscillations average to zero. Figure adapted from figure 1 of Reference 93. Copyright 2009 by the Institute of Physics.

eigenstate if (93)

$$|\omega - \hat{\mathbf{p}} \cdot \mathbf{K}| \gg |\vec{H}_{\nu\nu,\hat{\mathbf{p}}}|. \qquad 28.$$

Equation 28 gives the criterion for when neutrinos or antineutrinos drop out of the collective precession mode and begin to oscillate incoherently with respect to other neutrinos. The neutrinos or antineutrinos that drop out in this way have oscillation frequencies ω that are so different from the collective oscillation frequency that neutrino self-interaction is not strong enough to maintain the corresponding polarization vectors in collective precession.

With the replacements $\omega \to (\omega \cos 2\theta_v - \lambda)$ and $\vec{B} \to -\vec{L}$, the above discussion also applies to the case with a large λ. Including these replacements, Equation 28 indicates that collective precession is indeed suppressed when the number density of electrons is much larger than that of neutrinos.

6. COLLECTIVE NEUTRINO OSCILLATIONS IN SUPERNOVAE

6.1. Neutrino Oscillation Regimes

With the picture for neutrino oscillations developed above, we can utilize the strength of neutrino self-interaction to sketch out neutrino oscillation regimes (**Figure 9**). We focus the following discussion on the two-flavor mixing scenario with $|\Delta m^2| \simeq \Delta m^2_{\rm atm}$ and $\theta_v \simeq \theta_{13}$. We designate $R^-_{\rm coll}$ as the radius closest to the PNS where collective oscillations set in. Likewise $R^+_{\rm coll}$ is the outer radius where collective oscillations cease. In both the NH and IH cases, $R^+_{\rm coll}$ can be estimated from the condition

$$\sqrt{2} G_{\rm F} n_{\bar{\nu}_e}(R^+_{\rm coll}) \simeq \frac{\Delta m^2_{\rm atm}}{\langle E_{\bar{\nu}_e} \rangle}, \qquad 29.$$

where $n_{\bar{\nu}_e}(r)$ is the total number density of the antineutrinos at r that are initially $\bar{\nu}_e$ at the neutrino sphere and $\langle E_{\bar{\nu}_e} \rangle$ is the average energy of these antineutrinos. Here we use $\bar{\nu}_e$ as the representative neutrino species and $\frac{\Delta m^2_{\rm atm}}{\langle E_{\bar{\nu}_e} \rangle}$ as an estimate of the frequency spread of the neutrino spectrum.

In the NH case, assuming a fully synchronized neutrino system, $R^-_{\rm coll}$ is approximately where (*65*)

$$\sqrt{2} G_{\rm F} n_e(R^-_{\rm coll}) \simeq \Omega_{\rm sync}. \qquad 30.$$

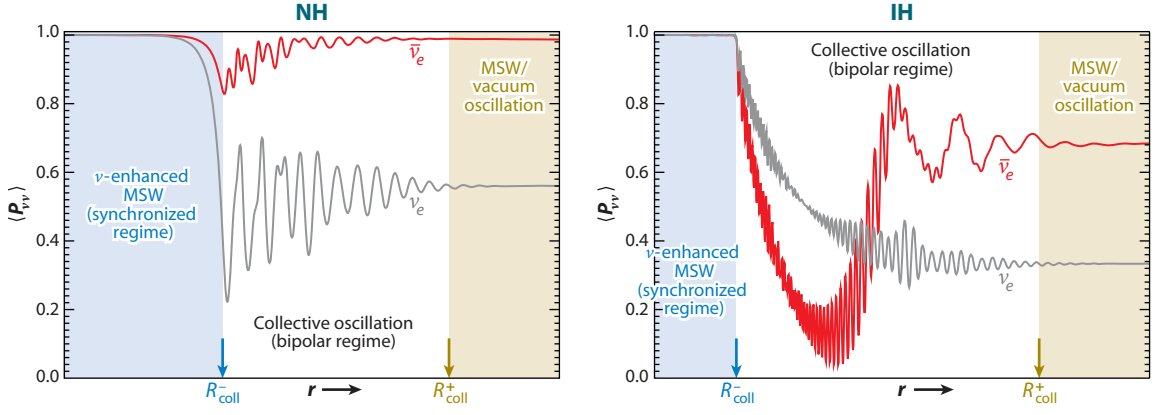

Figure 9

Schematic plots of the neutrino oscillation regimes in the core-collapse supernova environment in the two-flavor mixing scenario with $|\Delta m^2| \simeq \Delta m^2_{\rm atm}$. Near the protoneutron star (PNS), and in the synchronized regime ($r \lesssim R^-_{\rm coll}$), collective neutrino oscillations are suppressed by either the large matter density or the large neutrino fluxes themselves. In this regime neutrinos can still experience ν-enhanced Mikheyev-Smirnov-Wolfenstein (MSW) flavor transformation. Far away from the PNS ($r \gtrsim R^+_{\rm coll}$), where the neutrino fluxes are negligible, neutrinos experience either vacuum oscillations or conventional MSW flavor transformation, depending on the matter density and the energy of the neutrino. If $R^+_{\rm coll} > R^-_{\rm coll}$, then there is a window ($R^-_{\rm coll} \lesssim r \lesssim R^+_{\rm coll}$, known as the bipolar regime) where neutrinos experience collective neutrino oscillations and where spectral swaps/splits develop. The curves show the energy-averaged neutrino survival probabilities for electron neutrinos and antineutrinos in single-angle calculations that are chosen to be representative of some late-time supernova conditions.

[In the large neutrino flux limit, the behavior of a neutrino system experiencing ν-enhanced MSW flavor transformation is the same as that of a synchronized neutrino system (76).] We note that for an iron core–collapse supernova at early times and in the NH case, $R^{+}_{\rm coll} \leq R^{-}_{\rm coll}$, meaning that the collective neutrino oscillation regime does not exist. At later times in these models a collective neutrino oscillation regime can appear when the matter density becomes relatively small. In contrast, collective neutrino oscillations can occur at early epochs in an O-Ne-Mg core–collapse supernova (80) because the progenitors of these supernovae have relatively lower masses (8–12$M_{\odot}$), and therefore, after core bounce, the PNS has a dilute, lower-density envelope (126, 127).

In the IH case, the value of $R^{-}_{\rm coll}$ is the larger of the values extracted from the following two conditions:

$$n_{\bar{\nu}_e}(R^{-}_{\rm coll}) \simeq \frac{1}{(\sqrt{1+\varepsilon}-1)^2}\frac{\Delta m^2_{\rm atm}}{\sqrt{2}G_{\rm F}\langle E_{\bar{\nu}_e}\rangle} \quad \text{and} \quad n_{\bar{\nu}_e}(R^{-}_{\rm coll}) \simeq n_e(R^{-}_{\rm coll}). \qquad 31.$$

The first condition in Equation 31 is based on the flavor pendulum model (see Equation 17), and the second condition accords with the discussion in Section 5.1. In the very early epochs of an iron core–collapse supernova, the collective neutrino oscillation regime may not exist in the IH case because of the presence of a large matter density.

6.2. Effects of Collective Neutrino Oscillations

The supernova neutrino energy spectra can be dramatically modified by collective neutrino oscillations. Perhaps the most prominent feature to arise from collective neutrino oscillations is the spectral swap/split (e.g., **Figure 1**). Obtaining this feature can depend on supernova conditions. For example, the calculations used to produce **Figure 1** would give no spectral swap/split if the matter density were too large (78, 91).

When ν_e and $\bar{\nu}_e$ are the most abundant neutrino species at the neutrino sphere, some qualitative aspects of collective neutrino oscillations in supernovae can be understood by using the flavor pendulum model. In the IH case, the initial configuration of the flavor pendulum is near its highest position and is unstable when the neutrino flux is below some critical value. (See the discussion in Section 4.2.) This implies that collective neutrino oscillations and their effects on neutrino energy spectra are relatively insensitive to the matter density or the exact value of θ_{13}. In the NH case, however, the flavor pendulum would be near its stable configuration unless MSW flavor transformation displaces it from this position. As a result, collective neutrino oscillations and their effects depend on the efficiency of the ν-enhanced MSW flavor transformation. In turn, the efficiency of this flavor transformation is sensitive to both the matter profile and the value of θ_{13}. This general picture is confirmed by multiangle calculations (77). The results shown in Reference 77 suggest that it may be possible to resolve the neutrino mass hierarchy with an observed supernova neutrino signal, even if the absolute neutrino masses and/or θ_{13} are too small to be measured in the laboratory.

Neutrino signals detected at very early times after core bounce may be important probes of neutrino mixing. For iron core–collapse supernovae, the neutrino spectra at very early times are modified by the conventional MSW mechanism and can be easily calculated (128). For O-Ne-Mg core–collapse supernovae, however, the matter density is so low above the PNS that even at these very early times, where the ν_e luminosity can be very large ($\sim 10^{53}$ erg s^{-1}), collective neutrino oscillations can create step-like features (swaps/splits) in the observed neutrino energy spectra (80). If these features are observed in a galactic supernova neutrino burst, then they could serve as diagnostics of the neutrino mass hierarchy and, in the NH case, even provide a measure of θ_{13}.

However, the spectral swap/split phenomenon is sensitive to the neutrino luminosities and energy spectra at the neutrino sphere. Presently there are rather large uncertainties in these quantities, especially for the late-time supernova environment. Also, very large neutrino fluxes do not necessarily imply a large neutrino oscillation effect; indeed, in the IH case a larger neutrino luminosity pushes $R^{-}_{\rm coll}$ to a larger radius.

Of course, collective neutrino oscillations are not the only way that neutrinos may experience flavor transformation in supernovae. As in the Sun, in supernovae neutrinos can also experience the conventional MSW flavor transformation. However, the matter profile in supernovae may not be smooth (e.g., because of shocks or turbulence) near MSW resonance regions, which can produce some interesting phenomena (101, 129–135).

In principle, the alteration of supernova neutrino energy spectra by collective neutrino oscillations and/or other processes of neutrino flavor transformation could affect supernova dynamics, shock reheating, and nucleosynthesis in neutrino-heated ejecta (41, 48, 50, 108, 136). However, modeling of this physics in realistic supernova conditions is at present primitive.

7. SUMMARY AND OPEN ISSUES

In this review, we have discussed collective neutrino oscillations in a simple bipolar neutrino system, in homogeneous and isotropic neutrino gases, and in anisotropic neutrino gases. The simple bipolar neutrino system (described by the flavor pendulum) is the simplest of these scenarios and is solvable analytically. It can be used to understand many qualitative features of collective neutrino oscillations in supernovae. The single-angle scheme essentially treats supernova neutrinos as a homogeneous and isotropic gas, and adiabatic neutrino flavor transformation in such a gas can be used to understand the spectral swap/split phenomenon in the supernova environment. An anisotropic neutrino gas can possess unique characteristics (e.g., suppression of collective flavor oscillations by large matter density), which makes it an important target for study because realistic physical environments such as core-collapse supernovae can be highly anisotropic.

We have covered some of the basic properties of collective neutrino oscillations, with emphasis on the two-flavor mixing case. There is much about the collective neutrino oscillation phenomenon that remains to be understood. For example, in Section 4.1 we skipped over the adiabaticity condition when we discussed adiabatic neutrino flavor transformation. Adiabaticity criteria developed so far (79) are difficult to use in practice.

There are other open issues in our current understanding of collective neutrino oscillations in supernovae. For example, there can be multiple spectral swaps/splits in the final neutrino energy spectra (**Figure 10**) (78, 103, 105). The appearance of these features, however, depends on the luminosities and energy spectra of the different neutrino species at the neutrino sphere. This finding cannot be explained by a grand collective precession mode in which all neutrinos and antineutrinos participate. In a more recent paper (110), it was reported that qualitatively different results could appear in some collective neutrino oscillation scenarios, depending on whether two-flavor mixing or full three-flavor mixing is used. All of these discoveries point to the need for a systematic study of supernova neutrino oscillations with neutrino self-interaction and full three-flavor mixing at various supernova epochs in which neutrino luminosities and energy spectra can be different. Also, numerical simulations of supernova explosions have clearly shown that realistic supernova environments may be highly anisotropic and inhomogeneous (28, 30–37, 137). It would be interesting to see how density inhomogeneities arising from, for instance, shock waves and turbulence might affect collective neutrino oscillations. It remains a towering numerical challenge to integrate fully hydrodynamic, three-dimensional supernova models with calculations of neutrino oscillations that include neutrino self-interaction. However, such

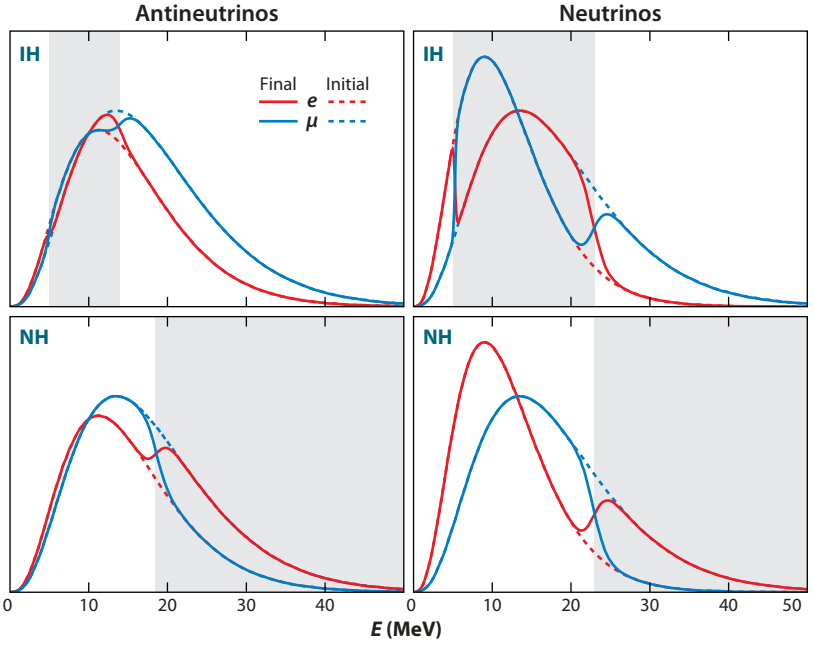

Figure 10

Multiple spectral swaps/splits in a two-flavor single-angle calculation with $|\Delta m^2| \simeq \Delta m^2_{\rm atm}$ and $\theta_{\rm v} \ll 1$. The solid and dashed curves represent the final and initial energy spectra, respectively. The red and blue curves are for e and μ flavors, respectively. The shaded regions mark the energy ranges in which spectral swaps occur. Unlike previous numerical calculations, this calculation assumes that ν_μ and $\bar{\nu}_\mu$, rather than ν_e and $\bar{\nu}_e$, are the most abundant neutrino species at the neutrino sphere. Abbreviations: IH, inverted neutrino mass hierarchy; NH, normal neutrino mass hierarchy. Reprinted with permission from Reference 103. Copyright 2009 by the American Physical Society.

self-consistent integration may be necessary to study the interplay between supernova physics and neutrino oscillations. Specifically, a full understanding of neutrino oscillations in supernovae may hold the key to deciphering the neutrino signal from a future galactic supernova. The stakes are high. Deciphering a supernova neutrino signal could provide important insights into supernova astrophysics. It could also provide key insights into fundamental neutrino properties, and such insights could be complementary to those sought by future neutrino experiments.

DISCLOSURE STATEMENT

The authors are not aware of any affiliations, memberships, funding, or financial holdings that might be perceived as affecting the objectivity of this review.

ACKNOWLEDGMENTS

We thank J. Carlson, J. Cherry, A. Friedland, W. Haxton, D. Kaplan, C. Kishimoto, A. Kusenko, A. Mezzacappa, and S. Reddy for useful conversations. We especially thank G. Raffelt for reading the manuscript and providing valuable comments. Our work was supported in part by the Institutional Computing Program at Los Alamos National Laboratory (LANL) and the National

Energy Research Scientific Computing Center, which is supported by the U.S. Department of Energy (DOE), Office of Science, under contract DE-AC02-05CH11231. Our work was also supported by DOE grant DE-FG02-00ER41132 at the Institute for Nuclear Theory; DOE grant DE-FG02-87ER40328 at the University of Minnesota; National Science Foundation grant PHY-06-53626 at the University of California, San Diego; and an Institute of Geophysics and Planetary Physics/LANL minigrant. The research of H.D. is supported by the LANL Laboratory Directed Research and Development program through the director's postdoctoral fellowship at LANL.

LITERATURE CITED

1. Camilleri L, Lisi E, Wilkerson JF. *Annu. Rev. Nucl. Part. Sci.* 58:343 (2008)
2. Timmes FX, Woosley SE, Weaver TA. *Astrophys. J. Suppl.* 98:617 (1995)
3. Abel T, Bryan GL, Norman ML. *Science* 295:93 (2002)
4. Samtleben D, Staggs S, Winstein B. *Annu. Rev. Nucl. Part. Sci.* 57:245 (2007)
5. Steigman G. *Annu. Rev. Nucl. Part. Sci.* 57:463 (2007)
6. Hannestad S. *Annu. Rev. Nucl. Part. Sci.* 56:137 (2006)
7. Fuller GM, Kishimoto CT. *Phys. Rev. Lett.* 102:201303 (2009)
8. Amsler C, et al. (Part. Data Group) *Phys. Lett.* B667:1 (2008)
9. Schwetz T, Tortola MA, Valle JWF. *New J. Phys.* 10:113011 (2008)
10. Mena O, Parke SJ. *Phys. Rev. D* 70:093011 (2004)
11. Guo X, et al. (Daya Bay Collab.) arXiv:hep-ex/0701029 (2007)
12. Bandyopadhyay A, et al. (ISS Phys. Work. Group) *Rep. Prog. Phys.* 72:106201 (2009)
13. Ray RE. *J. Phys. Conf. Ser.* 136:022019 (2008)
14. Terri R. (T2K Collab.) *Nucl. Phys. Proc. Suppl.* 189:277 (2009)
15. Adamson P, et al. (MINOS Collab.) *Phys. Rev. Lett.* 103:261802 (2009)
16. Fuller GM, Haxton WC, McLaughlin GC. *Phys. Rev. D* 59:085005 (1999)
17. Lunardini C, Smirnov AY. *J. Cosmol. Astropart. Phys.* 0306:009 (2003)
18. Beacom JF, Vagins MR. *Phys. Rev. Lett.* 93:171101 (2004)
19. Cadonati L, Calaprice FP, Chen MC. *Astropart. Phys.* 16:361 (2002)
20. Ahrens J, et al. (AMANDA Collab.) *Astropart. Phys.* 16:345 (2002)
21. Sharp MK, Beacom JF, Formaggio JA. *Phys. Rev. D* 66:013012 (2002)
22. Ikeda M, et al. (Super-Kamiokande Collab.) *Astrophys. J.* 669:519 (2007)
23. Autiero D, et al. *J. Cosmol. Astropart. Phys.* 0711:011 (2007)
24. Colgate SA, Grasberger WH, White RH. *Astron. J.* 66:280 (1961)
25. Woosley SE, Heger A, Weaver TA. *Rev. Mod. Phys.* 74:1015 (2002)
26. Woosley S, Janka T. *Nat. Phys.* 1:147 (2005)
27. Janka H-T, et al. *Phys. Rep.* 442:38 (2007)
28. Herant M, et al. *Astrophys. J.* 435:339 (1994)
29. Burrows A, Hayes J, Fryxell BA. *Astrophys. J.* 450:830 (1995)
30. Buras R, Rampp M, Janka HT, Kifonidis K. *Astron. Astrophys.* 447:1049 (2006)
31. Bruenn SW, et al. *J. Phys. Conf. Ser.* 46:393 (2006)
32. Ott CD, Burrows A, Dessart L, Livne E. *Astrophys. J.* 685:1069 (2008)
33. Hammer NJ, Janka HT, Mueller E. *Astrophys. J.* 714:1371 (2010)
34. Murphy JW, Burrows A. *Astrophys. J.* 688:1159 (2008)
35. Bruenn SW, et al. *J. Phys. Conf. Ser.* 180:012018 (2009)
36. Blondin JM, Mezzacappa A. *Astrophys. J.* 642:401 (2006)
37. Blondin JM, Mezzacappa A. *Nature* 445:58 (2007)
38. Bethe HA, Wilson JR. *Astrophys. J.* 295:14 (1985)
39. Bethe HA. *Rev. Mod. Phys.* 62:801 (1990)
40. Arnett D. *Supernovae and Nucleosynthesis*. Princeton: Princeton Univ. Press (1996)
41. Qian Y-Z, et al. *Phys. Rev. Lett.* 71:1965 (1993)
42. Horowitz CJ. *Phys. Rev. D* 65:043001 (2002)

43. Prakash M, Lattimer JM, Sawyer RF, Volkas RR. *Annu. Rev. Nucl. Part. Sci.* 51:295 (2001)
44. Wolfenstein L. *Phys. Rev. D* 17:2369 (1978)
45. Mikheyev SP, Smirnov AY. *Yad. Fiz.* 42:1441 (1985)
46. Fuller GM, Mayle RW, Wilson JR, Schramm DN. *Astrophys. J.* 322:795 (1987)
47. Nötzold D, Raffelt GG. *Nucl. Phys. B* 307:924 (1988)
48. Fuller GM, Mayle RW, Meyer BS, Wilson JR. *Astrophys. J.* 389:517 (1992)
49. Fuller GM. *Phys. Rep.* 227:149 (1993)
50. Qian Y-Z, Fuller GM. *Phys. Rev. D* 51:1479 (1995)
51. Qian Y-Z, Fuller GM. *Phys. Rev. D* 52:656 (1995)
52. Pantaleone JT. *Phys. Rev. D* 46:510 (1992)
53. Pantaleone JT. *Phys. Lett.* B287:128 (1992)
54. Samuel S. *Phys. Rev. D* 48:1462 (1993)
55. Kostelecký VA, Pantaleone JT, Samuel S. *Phys. Lett.* B315:46 (1993)
56. Kostelecký VA, Samuel S. *Phys. Lett.* B318:127 (1993)
57. Kostelecký VA, Samuel S. *Phys. Rev. D* 49:1740 (1994)
58. Kostelecký VA, Samuel S. *Phys. Rev. D* 52:621 (1995)
59. Samuel S. *Phys. Rev. D* 53:5382 (1996)
60. Kostelecký VA, Samuel S. *Phys. Lett.* B385:159 (1996)
61. Pantaleone JT. *Phys. Rev. D* 58:073002 (1998)
62. Pastor S, Raffelt GG, Semikoz DV. *Phys. Rev. D* 65:053011 (2002)
63. Dolgov AD, et al. *Nucl. Phys. B* 632:363 (2002)
64. Abazajian KN, Beacom JF, Bell NF. *Phys. Rev. D* 66:013008 (2002)
65. Pastor S, Raffelt GG. *Phys. Rev. Lett.* 89:191101 (2002)
66. Balantekin AB, Yüksel H. *New J. Phys.* 7:51 (2005)
67. Fuller GM, Qian Y-Z. *Phys. Rev. D* 73:023004 (2006)
68. Duan H, Fuller GM, Qian Y-Z. *Phys. Rev. D* 74:123004 (2006)
69. Duan H, Fuller GM, Carlson J, Qian Y-Z. *Phys. Rev. Lett.* 97:241101 (2006)
70. Duan H, Fuller GM, Carlson J, Qian Y-Z. *Phys. Rev. D* 74:105014 (2006)
71. Hannestad S, Raffelt GG, Sigl G, Wong YYY. *Phys. Rev. D* 74:105010 (2006)
72. Raffelt GG, Sigl G. *Phys. Rev. D* 75:083002 (2007)
73. Duan H, Fuller GM, Carlson J, Qian Y-Z. *Phys. Rev. D* 75:125005 (2007)
74. Raffelt GG, Smirnov AY. *Phys. Rev. D* 76:081301(R) (2007)
75. Esteban-Pretel A, et al. *Phys. Rev. D* 76:125018 (2007)
76. Duan H, Fuller GM, Qian Y-Z. *Phys. Rev. D* 76:085013 (2007)
77. Duan H, Fuller GM, Carlson J, Qian Y-Z. *Phys. Rev. Lett.* 99:241802 (2007)
78. Fogli GL, Lisi E, Marrone A, Mirizzi A. *J. Cosmol. Astropart. Phys.* 0712:010 (2007)
79. Raffelt GG, Smirnov AY. *Phys. Rev. D* 76:125008 (2007)
80. Duan H, Fuller GM, Carlson J, Qian Y-Z. *Phys. Rev. Lett.* 100:021101 (2008)
81. Esteban-Pretel A, et al. *Phys. Rev. D* 77:065024 (2008)
82. Lunardini C, Mueller B, Janka HT. *Phys. Rev. D* 78:023016 (2008)
83. Dasgupta B, Dighe A. *Phys. Rev. D* 77:113002 (2008)
84. Duan H, Fuller GM, Qian Y-Z. *Phys. Rev. D* 77:085016 (2008)
85. Dasgupta B, Dighe A, Mirizzi A, Raffelt GG. *Phys. Rev. D* 77:113007 (2008)
86. Dasgupta B, Dighe A, Mirizzi A. *Phys. Rev. Lett.* 101:171801 (2008)
87. Duan H, Fuller GM, Carlson J. *Comput. Sci. Disc.* 1:015007 (2008)
88. Sawyer RF. *Phys. Rev. D* 79:105003 (2009)
89. Chakraborty S, Choubey S, Dasgupta B, Kar K. *J. Cosmol. Astropart. Phys.* 0809:013 (2008)
90. Dasgupta B, Dighe A, Mirizzi A, Raffelt GG. *Phys. Rev. D* 78:033014 (2008)
91. Esteban-Pretel A, et al. *Phys. Rev. D* 78:085012 (2008)
92. Gava J, Volpe C. *Phys. Rev. D* 78:083007 (2008)
93. Duan H, Fuller GM, Qian Y-Z. *J. Phys. G* 36:105003 (2009)
94. Raffelt GG. *Phys. Rev. D* 78:125015 (2008)
95. Blennow M, Mirizzi A, Serpico PD. *Phys. Rev. D* 78:113004 (2008)

96. Fogli G, Lisi E, Marrone A, Tamborra I. *J. Cosmol. Astropart. Phys.* 0904:030 (2009)
97. Lunardini C, Peres OLG. *J. Cosmol. Astropart. Phys.* 0808:033 (2008)
98. Guo X-H, Huang M-Y, Young B-L. *Phys. Rev. D* 79:113007 (2009)
99. Minakata H, Nunokawa H, Tomas R, Valle JWF. *J. Cosmol. Astropart. Phys.* 0812:006 (2008)
100. Liao W. arXiv:0904.0075 [hep-ph] (2009)
101. Duan H, Kneller JP. *J. Phys. G* 36:113201 (2009)
102. Liao W. arXiv:0904.2855 [hep-ph] (2009)
103. Dasgupta B, Dighe A, Raffelt GG, Smirnov AY. *Phys. Rev. Lett.* 103:051105 (2009)
104. Galais S, Kneller J, Volpe C, Gava J. *Phys. Rev. D* 81:053002 (2010)
105. Fogli G, Lisi E, Marrone A, Tamborra I. *J. Cosmol. Astropart. Phys.* 0910:002 (2009)
106. Esteban-Pretel A, Tomas R, Valle JWF. *Phys. Rev. D* 81:063003 (2010)
107. Gava J, Kneller J, Volpe C, McLaughlin GC. *Phys. Rev. Lett.* 103:071101 (2009)
108. Chakraborty S, Choubey S, Goswami S, Kar K. arXiv:0911.1218 [hep-ph] (2009)
109. Lazauskas R, Lunardini C, Volpe C. *J. Cosmol. Astropart. Phys.* 0904:029 (2009)
110. Friedland A. *Phys. Rev. Lett.* 104:191102 (2010)
111. Gava J, Jean-Louis CC. arXiv:0912.5206 [hep-ph] (2009)
112. Balantekin AB, Fuller GM. *Phys. Lett.* B471:195 (1999)
113. Caldwell DO, Fuller GM, Qian Y-Z. *Phys. Rev. D* 61:123005 (2000)
114. Sigl G, Raffelt GG. *Nucl. Phys. B* 406:423 (1993)
115. McKellar BHJ, Thomson MJ. *Phys. Rev. D* 49:2710 (1994)
116. Strack P, Burrows A. *Phys. Rev. D* 71:093004 (2005)
117. Halprin A. *Phys. Rev. D* 34:3462 (1986)
118. Bell NF, Rawlinson AA, Sawyer RF. *Phys. Lett.* B573:86 (2003)
119. Friedland A, Lunardini C. *J. High Energy Phys.* 10:043 (2003)
120. Sawyer RF. *Phys. Rev. D* 72:045003 (2005)
121. Friedland A, McKellar BHJ, Okuniewicz I. *Phys. Rev. D* 73:093002 (2006)
122. Balantekin AB, Pehlivan Y. *J. Phys. G* 34:47 (2007)
123. Kim CW, Kim J, Sze WK. *Phys. Rev. D* 37:1072 (1988)
124. Duan H. *AIP Conf. Proc.* 1182:36 (2009)
125. Cardall CY. *Phys. Rev. D* 78:085017 (2008)
126. Nomoto K. *Astrophys. J.* 277:791 (1984)
127. Nomoto K. *Astrophys. J.* 322:206 (1987)
128. Kachelriess M, et al. *Phys. Rev. D* 71:063003 (2005)
129. Sawyer RF. *Phys. Rev. D* 42:3908 (1990)
130. Loreti FN, Qian Y-Z, Fuller GM, Balantekin AB. *Phys. Rev. D* 52:6664 (1995)
131. Schirato RC, Fuller GM. arXiv:astro-ph/0205390 (2002)
132. Fogli GL, Lisi E, Montanino D, Mirizzi A. *Phys. Rev. D* 68:033005 (2003)
133. Kneller JP, McLaughlin GC. *Phys. Rev. D* 73:056003 (2006)
134. Friedland A, Gruzinov A. arXiv:astro-ph/0607244 (2006)
135. Dasgupta B, Dighe A. *Phys. Rev. D* 75:093002 (2007)
136. Sigl G. *Phys. Rev. D* 51:4035 (1995)
137. Fryer CL, Warren MS. *Astrophys. J.* 574:L65 (2002)

Annual Review of Nuclear and Particle Science

Volume 60, 2010

Contents

Indexes

Errata

An online log of corrections to *Annual Review of Nuclear and Particle Science* articles may be found at http://nucl.annualreviews.org/errata.shtml